123. G. A. Brucker, S. I. Ionov, Y. Chen and C. Wittig, *Chem. Phys. Lett.* **194**, 301 (1992).
124. K. W. D. Ledingham, C. Kosmidis, S. Georgiou, S. Couris and R. P. Singhal, *Chem. Phys. Lett.* **247**, 555 (1995).
125. K. Vijayalakshmi, C. P. Safvan, G. Ravinda Kumar and D. Mathur, *Chem. Phys. Lett.* **270**, 37 (1997).
126. R. E. Continetti, *Int. Rev. Phys. Chem.* **17**, 227 (1998).
127. K. S. Haber, J. W. Zwanziger, F. X. Campos, R. T. Wiedmann and E. R. Grant, *Chem. Phys. Lett.* **144**, 58 (1988).
128. Y. Arasaki, K. Takatsuka, K. Wang and V. McKoy, *Chem. Phys. Lett.* **302**, 363 (1999).
129. T. Zuo, A. D. Bandrauk and P. B. Corkum, *Chem. Phys. Lett.* **259**, 313 (1996).
130. K. Wang, V. McKoy and H. Rudolph, *Chem. Phys. Lett.* **216**, 490 (1994).
131. I. Powis, *Chem. Phys.* **201**, 189 (1995); I. Powis, *J. Chem. Phys.* **106**, 5013 (1997).
132. W. G. Roeterdink and M. H. M. Janssen, *Chem. Phys. Lett.* **345**, 72 (2001).
133. W. G. Roeterdink and M. H. M. Janssen, *Phys. Chem. Chem. Phys.* **4**, 601 (2001).
134. A. M. Rijs, C. C. Hayden and M. H. M. Janssen, in *Femtochemistry and Femtobiology: Ultrafast Dynamics in Molecular Science*, ed. A. Douhal and J. Santamaria (World Scientific Publishing Co. Pte. Ltd., Singapore, 2002) p. 91.
135. K. G. Low, P. D. Hampton and I. Powis, *Chem. Phys.* **100**, 401 (1985).
136. P. Downie and I. Powis, *J. Chem. Phys.* **111**, 4535 (1999).
137. T. G. Clements and R. E. Continetti, *Phys. Rev. Lett.* **89**, 033005-1–033005-4 (2002).

CHAPTER 12

TIME-RESOLVED PHOTOELECTRON SPECTROSCOPY AND IMAGING

Toshinori Suzuki
Chemical Dynamics Laboratory, RIKEN, Wako, 351-0198 Japan and Japan Science and Technology Corporation, 332-0012 Japan

Contents

1. Introduction

Ultraviolet photoelectron spectroscopy (UV-PES) was developed by Turner,[1] Vilesov[2] and their coworkers in the early 1960s. The method played an important role in chemistry for establishing a molecular orbital picture of electronic states. The well-known Koopmans' theorem[3] provides a direct link between the ionization energy and the orbital energy calculated at the Hartree–Fock level: if removal of an electron does not affect any other occupied orbital, the ionization energy directly provides the negative value of the orbital energy, i.e. $I_j = -\varepsilon_j$. Although this relation is only approximate, because a single determinant self-consistent field picture is inaccurate,[4] a large body of information on molecular orbitals was obtained by He(I) one-photon ionization PES.[5–9]

Pump-probe photoelectron spectroscopy is a variant of resonance enhanced multi-photon ionization photoelectron spectroscopy (REMPI-PES) made possible by high-intensity lasers.[10–12] In one-color REMPI-PES of molecules initiated in the 1980s, ionizations from dark states populated by non-radiative processes from optically-excited bright states were sometimes identified.[12–14] These observations clearly indicated that PES can be used to elucidate not only the static electronic structure of a molecule, as demonstrated by UV-PES and Koopmans' theorem, but also dynamics of the non-stationary state created by an optical excitation. One-color REMPI-PES is similar in nature to dispersed fluorescence spectroscopy (DF), as these are unfolded and folded forms of two sequential electronic transitions. However, one-color REMPI-PES provides a shorter time-gate for observation than DF, since the former is only limited by the laser pulse duration, while the latter is limited by the emission lifetime of the excited state. Time-resolved photoelectron spectroscopy (TRPES) is based on a two-color pump-probe scheme where laser pulse durations are much shorter than the characteristic time of the dynamics of interest and the photoelectron scattering distributions are observed as a function of the pump-probe time delay. Its time-resolution has been improved from nanoseconds in the 1980s down to a few tens of femtoseconds in the last decade,[15–20] due to the advent of solid-state ultrafast lasers and non-linear optical technologies.[21]

It is noted that the directional properties of the bound state orbitals and outgoing scattering waves upon ionization are never known from photoelectron kinetic energy distributions (PEDs). Photoelectron angular distributions (PADs), if possible measured in the molecular frame (MF), are

indispensable for their elucidation. In the past, PAD measurements were extremely time-consuming. For this reason, Turner and coworkers have proposed, thirty years ago, using two detectors for observing electrons scattered parallel and perpendicular to the light polarization (Fig. 1), to allow routine determination of angular anisotropy parameters in a one-photon ionization process.[22] Photoelectron imaging (PEI)[23–33] is an advanced form of the multiplex detection of electrons in the same spirit as the method proposed by Turner and coworkers, and it enables extremely accurate and reliable measurements of PADs. Time-resolved photoelectron imaging (TRPEI)[34–39] described in the present chapter opens new opportunities for exploring excited state dynamics and elucidating photoionization stereodynamics. The particular topic of photoelectron and photoion coincidence is discussed only briefly in the present chapter to avoid duplication with other chapters of this book.

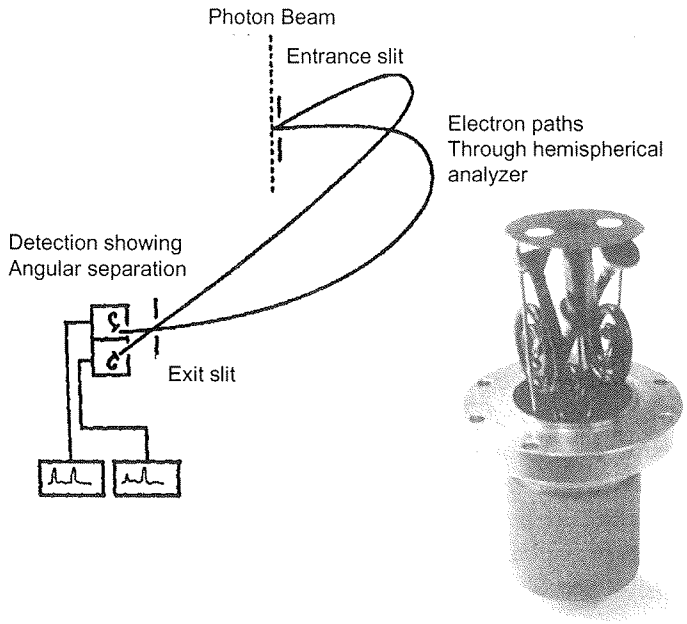

Fig. 1. Multiplex detection of a photoelectron angular distribution using two channeltrons proposed by Turner and coworkers in 1972. Reproduced with permission from Ref. 22.

2. Photoionization Probing of Non-Stationary States: Basic Ideas

Coherent excitation of an ensemble of eigenstates creates a non-stationary state or a wave-packet.[40] Since cross sections for ionization from this non-stationary state to various final states, i.e. different cationic rovibronic states and photoelectron scattering partial waves, vary with the time-dependent phase factors of these component states, TRPES allows observation of electronic, vibrational and rotational wave-packets of a molecular system.

Let us imagine a potential energy curve crossing between a covalent (AB) and an ion pair state (A^+B^-) in a heteronuclear diatomic molecule. Ionization from the latter state may occur to the cationic state with a strong (A^+B) character, whereas ionization from the former may lead to both (AB^+) and (A^+B) states. Therefore, a vibrational wave-packet motion may change the ionization signal leading to different cationic states of (AB^+) and (A^+B), provided that cationic electronic states have distinct electronic configurations. Such an idea was presented by Engel and coworkers,[41,42] who proposed pump-probe mass spectrometry on NaI, where they predicted that photoionization from the inner and outer turning points on the excited state potential energy curve formed by the covalent-ionic curve crossing should produce different ionic products. Later, Engel and coworkers also calculated the photoelectron energy spectra for a pump-probe photoionization experiment of NaI.[43,44] These proposals were tested experimentally by Jouvet and coworkers.[45] Charron and Suzor-Weiner refined the theoretical analysis on the system.[46] (The predicted behavior of an ionization branching ratio in this particular system was unfortunately not observed or calculated in these studies.[45–46])

Even if ionization occurs from a non-stationary state to a single cationic electronic state, vibrational wave-packet motion can be monitored from the photoelectron kinetic energies (PKEs) that vary as a function of pump-probe time delay. As the vibrational wave-packet oscillates on the adiabatic potential energy curve, it sees variations of the vertical ionization energy depending on the internuclear distance. Therefore, the vibrational wave-packet motion modulates PKEs. Baumert and coworkers have studied vibrational wave-packet dynamics in the $2^1\Pi_g$ state of Na_2 prepared by two-photon absorption from the ground state via the $A^1\Sigma_u^+$ state.[47] As the vibrational wave-packet moves back and forth between the inner and outer turning points on the $2^1\Pi_g$ potential, the

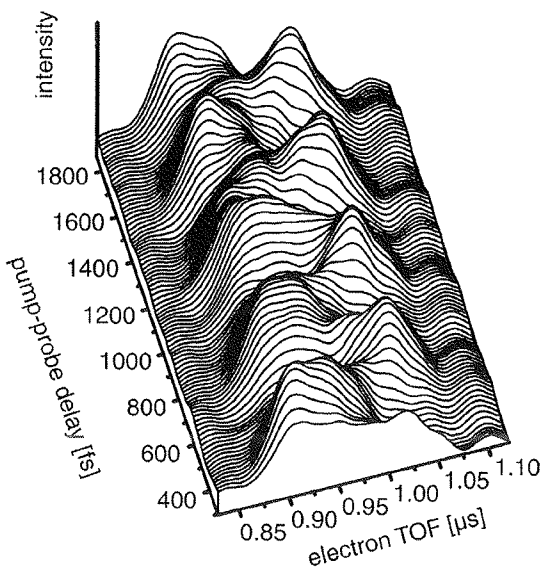

Fig. 2. Vibrational wave-packet motion in the $2^1\Pi_g$ state of Na_2 probed by TRPES. Reproduced with permission from Ref. 47.

PKE exhibits oscillatory features reflecting the wave-packet dynamics[47] (Fig. 2).

A number of TRPES experiments were performed on aromatic molecules. In these systems, the complex multi-dimensional nature and high vibrational frequencies did not allow clear observation of vibrational wave-packet dynamics, but rather the overall change of vibrational energy upon electronic dephasing. Since aromatic molecules have rigid frameworks, geometrical changes upon electronic excitation and ionization are small, resulting in Franck–Condon factors dominated by $\Delta v = 0$ transitions. When electronic dephasing occurs from an optically bright (S) state to a dark electronic state(s) (T), and when these two states are ionized to the same cationic electronic state, the S–T energy difference is transformed into the vibrational energy in the T state, since the total energy must be conserved under collision free conditions. Subsequently, this vibrational energy is approximately conserved upon photoionization, resulting in PKEs that shift upon electronic dephasing towards a lower value roughly equal to the S–T energy gap. Another important dynamical process in large molecules is intramolecular vibrational energy redistribution (or vibrational dephasing) within one electronic state. Intramolecular vibrational energy redistribution

(IVR) occurs from a bright vibrational state to an ensemble of dark background states that are typically combination and overtone of low-frequency modes. An ionization process from the bath states after IVR approximately conserves the vibrational energy, so its spectral features resemble that of the photoelectron spectrum from the zero vibrational level in the excited state, except for the broadening of the bands: this is analogous to the well-known results in dispersed fluorescence spectroscopy on alkyl-benzene by Smalley and coworkers.[48–50] TRPES shares various features with the time-resolved dispersed fluorescence or stimulated emission pumping spectroscopies, as these are folded and unfolded forms of two-color electronic spectroscopy.

If the orientation of a molecule is defined, the change of electronic state may be detected from the PAD in the molecular frame (MF-PAD). If we consider the curve crossing in the AB molecule, ionization from the ion pair state to the AB^+ state may eject a photoelectron from the B atom side, whereas ionization leading to A^+B may lead to ejection from the A side. The possibility of MF-PAD measurements has been demonstrated previously in one-photon ionization experiments. Heinzmann and coworkers oriented gaseous CH_3I using a hexapole state selector and measured the photoelectrons generated by VUV light in the direction parallel and anti-parallel to the orientation field.[51] They observed an asymmetry in the PAD that indicated primarily electron emission from the iodine end of the molecule. Golovin,[52–54] Yagishita[55–61] and their coworkers have employed a photoelectron-photoion coincidence (PEPICO) technique in conjunction with dissociative ionization to measure MF-PADs. In these experiments, a small molecule is dissociatively ionized, then a photoelectron is ejected and the molecular ion core immediately breaks apart. If the ion dissociates within its rotational time period, the fragments are, in the case of a two-body dissociation, ejected along the molecular axis (axial recoil approximation).[62–78] One can then measure the angular correlation between the recoil velocities of the ion and the electron to obtain the MF-PAD. These experiments clearly indicate the feasibility of pump-probe MF-PAD measurements to explore the evolution of molecular orbitals during the course of a chemical reaction, although its application is limited to small molecules due to requirement of instantaneous dissociation upon ionization. Hayden and coworkers have presented the first example of MF-PAD measurements in conjunction with a femtosecond pump-probe scheme quite recently.[38,39] Further developments are anticipated in the area.

3. REMPI-PES and Electron Configuration Interactions

In a one-photon transition, two-electron excitation is less likely than one-electron excitation. Therefore, to a first order approximation, ionization is expected to leave an ion core with an electron removed from one of the occupied orbitals with all other occupancies unchanged. Then, PES may be used to probe occupancies of molecular orbitals and configuration interactions. On the other hand, since REMPI-PES probes ionization from the excited states of molecules, considerations of configuration interactions (CI) become more important than in one-photon ionization from the ground state. Therefore, even if the one-electron approximation holds, ionization cross sections from a particular neutral state to various cationic states should be predicted with caution.

De Lange and coworkers have observed $(2+1)$ REMPI-PES of the SH radical via the $4p\sigma(^2\Sigma^+)$ Rydberg state with $[b^1\Sigma^+]$ ion core.[79,80] However, additional peaks observed in the spectrum were assigned to ionization to the $a^1\Delta$ state of the cation, indicating that the $[b^1\Sigma^+]4p\sigma^2\Sigma^+$ state is interacting with another $^2\Sigma^+$ $(v'=1)$ Rydberg state with $[a^1\Delta]$ ion core. With this in mind, they searched for the perturber and found a candidate at $\sim 800\,\mathrm{cm}^{-1}$ higher in energy than the $[b^1\Sigma^+]4p\sigma^2\Sigma^+$ $(v'=0)$ state. The photoelectron spectra observed on ionization from this state, exhibited $[b^1\Sigma^+]$ character in addition to the feature arising from the $[a^1\Delta]$ $(v'=1)$ Rydberg state, and it has been assigned to the $[a^1\Delta]3d\delta^2\Sigma^+$ $(v'=1)$ state.[79,80] This is a favorable case of probing state mixing by REMPI-PES, since ionization cross sections from the Rydberg states to the cationic states show a clear propensity of preserving the ion core.

In their pioneering studies on nanosecond REMPI-PES, Kimura, Achiba and coworkers have investigated the $S_2 - S_1$ internal conversion in naphthalene[14] and the $S_2 - T_1$ intersystem crossing in isoquinoline.[81] In the latter work, they attempted to discriminate between the $^3(n,\pi^*)$ and $^3(\pi,\pi^*)$ states, possibly involved in the intersystem crossing, based on the one-electron approximation: ionization from the $^3(\pi,\pi^*)$ is expected to reach a π^{-1} cationic state with an electron hole in the π orbital, whereas ionization from the $^3(n,\pi^*)$ state should lead to n^{-1}. From their PES results, they speculated that $^3(n,\pi^*)$ is located between the S_2 $^1(\pi,\pi^*)$ and T_1 $^3(\pi,\pi^*)$ states.[81] The validity of this type of argument depends largely on the extent of configuration interaction among the excited states, rather than on the accuracy of one-electron propensity rule in a one-photon transition. Due to the advent of molecular orbital and density functional calculations

along with enhanced computational power in the last decade, it became feasible to computationally examine configuration interactions in the excited states to predict the ionization cross sections to different cationic states at least semi-quantitatively.[82]

Stolow and coworkers have shown that ionizations from the S_2 and S_1 states of *all-trans* 2,4,6,8-decatetraene occur to different electronic states of the cation,[83,84] while they reach the same cationic electronic state in phenanthrene and naphthalene.[85] The semi-empirical QCDD/PI+CISD method was used to analyze electron configurations of neutral excited states and cationic states to obtain relative ionization cross sections. In decatetraene, the S_2 state arises from an almost pure, 95%, HOMO($2b_g$)-LUMO($3a_u$) transition and is correlated to D_0. Various electron configurations including a well-known two-electron excitation in polyenes contribute to the S_1 state, which enables ionization from S_1 to both D_0 and D_1.[84] In phenanthrene, both S_1 and S_2 states have considerable contributions from different electron configurations, resulting in ionization into D_0 and D_1 with similar cross sections.[85]

4. Brief Overview of Time-Resolved Photoelectron (Energy) Spectroscopy

4.1. *Radiationless Transitions*

TRPES dates back, at least, to the mid 1980s, with observations of radiationless transitions in triazine[86] and benzene.[87] Weber and Thantu have performed one-color (1 + 1) picosecond TRPES experiments on azulene and phenanthrene.[88] The observed spectral features varied with laser pulse duration, indicating the existence of internal conversion processes to lower states in these systems.

Kim, Schick and Weber performed more extensive two-color picosecond TRPES on aniline, 2-aminopyridine, and 3-aminopyridine.[82] Their spectra, shown in Fig. 3, exhibit a generic feature of TRPES upon electronic dephasing in an isolated molecule. The spectrum (a) measured with a time delay <50 ps shows a distinct vibrational feature corresponding to ionization from S_1, whereas a broad distribution gradually appears at later times, in (b) and (c), due to ionization from the dark triplet manifold. There were two possible explanations for ionization from the triplet state to show the shift in PKE. One possibility was that the electron configuration in the triplet state provided a large ionization cross section reaching the excited state of the cation, with virtually no transition probability to the ground

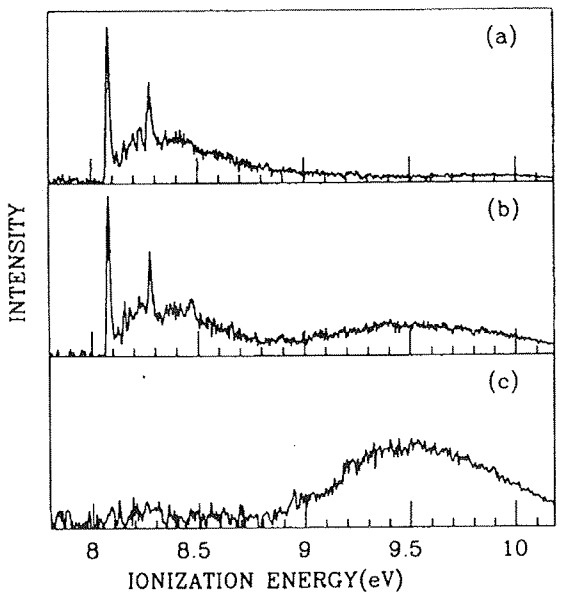

Fig. 3. Time-resolved PED in (1 + 1′) picosecond TRPES of 3-aminopyridine via the S_1 zero vibrational state. The time delays are (a) <50 ps, (b) 0.5 ns, and (c) 2 ns. The broad distribution is due to ionization from the T_1 state after intersystem crossing from S_1. Reproduced with permission from Ref. 82.

ionic state. The other was that the electronic energy difference between S_1 and the triplet state was transformed into vibrational energy in the triplet, which was conserved upon photoionization. In order to discriminate between these two possibilities, Kim *et al.* have performed INDO/1 molecular orbital calculations to estimate the term values and the electron configurations of the triplet states. Then, the one-electron approximation was invoked to predict the cationic electronic state reached by ionization from each triplet state. The $\Delta v = 0$ propensity rule was assumed for the Franck–Condon factor. From this analysis, they concluded that intersystem crossing from S_1 occurred only to T_1 in all of these three molecules, even though the T_2 and T_3 states were energetically accessible, and ionization occurs to D_0. They demonstrated convincingly that considerations of configuration interaction in neutral excited states, ionization cross sections, and plausible assignments of dark states are quite important in TRPES. The same group has also performed femtosecond TRPES *via* S_1 and S_2 states of Phenol.[89]

Reilly,[90] Knee,[91] and their coworkers have explored IVR in excited states by picosecond TRPES. In the former work,[90] *p*-*n*-alkylanilines were excited to the S_1 1^1 vibronic level, and photoelectron spectra were measured by time-delayed picosecond pulses. The sharp structure due to ionization from the zero-order 1^1 level diminished in time and a broadened feature appeared due to ionization from dark bath states formed by low-frequency vibrational modes associated with the alkyl chain. The observed IVR rates were found to be dependent on the length and the conformation of the alkyl chains, in agreement with the results by Smalley,[92] Zewail[93] and their coworkers. Knee and coworkers have excited fluorene molecules to S_1 vibronic levels with vibrational energies of 834 and 1707 cm^{-1} and recorded the photoelectron spectra by pulsed field ionization zero kinetic energy (PFI-ZEKE) photoelectron spectroscopy.[91] The PFI-ZEKE method[94–96] is useful to obtain a high-resolution photoelectron spectrum in conjunction with picosecond lasers with an energy resolution of 5–10 cm^{-1}: in the femtosecond time range, the advantage of high-resolution PFI-ZEKE diminishes due to unavoidable energy broadening arising from the uncertainty principle. Knee and coworkers observed quantum beats as the signature of restricted IVR from the 834 cm^{-1} level, whereas dissipative IVR behavior was seen for the 1707 cm^{-1} level.[91] These observations were in agreement with a previous study by McDonald and coworkers on the same molecule with time-resolved fluorescence depletion (analogous to time-resolved stimulated emission pumping) method.[97,98] Smith, Zhang and Knee have applied picosecond PFI-ZEKE to explore IVR and vibrational predissociation in the S_1 state of the aniline-CH_4 van der Waals (vdW) complex[99] and the well-known channel three problem in benzene.[100]

De Lange and coworkers have employed picosecond TRPES to study the A band photodissociation of CH_3I,[101] and the predissociative $B(^1E'')$ and $C'(^1A_1')$ states of NH_3.[102] Fischer and coworkers used TRPES to measure the lifetimes of vibrational levels in the B, C, and D excited states of the allyl radical: TRPES showed that these states disappear within 20 ps due to internal conversion to the ground state.[103,104] This work is notable as an application of TRPES to reactive species.

Seel and Domcke reported a seminal theoretical study on femtosecond TRPES, in which they considered photoionization probing of the $S_2(\pi,\pi^*)$–$S_1(n,\pi^*)$ ultrafast internal conversion (IC) in pyrazine.[105–109] Historically, this system attracted much attention from theorists and experimentalists, since due to the high symmetry (D_{2h}) of the molecule the vibronic coupling between the two electronic states is induced by only one

vibrational mode 10a. The S_2 and S_1 potential energy surfaces form a conical intersection with the modes 10a and 6a. Seel and Domcke examined two possible situations for (1 + 1′) REMPI of pyrazine: (a) S_1 and S_2 are ionized to $D_0(n^{-1})$ and $D_1(\pi^{-1})$, respectively; and (b) both S_1 and S_2 are ionized to D_0. Hahn and Stock have also treated TRPES of this system theoretically.[110] On the other hand, a corresponding experimental investigation has not been fully realized, mainly due to the fact that the $S_2(\pi,\pi^*) \rightarrow S_1(n,\pi^*)$ IC is extremely fast, $\tau = 30$ fs. Radloff and coworkers have addressed this problem with somewhat long, 130 fs, laser pulses at 267 nm and 200 nm.[111] The pump-probe ion signal was deconvoluted to obtain the S_2–S_1 IC rate of 20 fs. The spectrum measured at $\delta t = 300$ fs is regarded as the photoelectron spectrum on ionization from S_1 after the ultrafast IC. They suggested that the difference between the two spectra measured at 0 and 300 fs was due to ionization from S_2, while the wavepacket is localized at the Franck–Condon region reached by one-photon excitation from S_0.

Cyr and Hayden applied femtosecond TRPES to $S_2(1^1B_u) - S_1(2^1A_g)$ IC in 1,3,5-hexatriene.[112]

4.2. *Wave-Packet Dynamics and Reactions*

One of the best-known achievements of real-time transition state spectroscopy or "stroboscopy" is pump-probe laser-induced fluorescence (LIF) of NaI[113–115] by Zewail and coworkers, where vibrational wave-packet motion and non-adiabatic transitions were clearly observed. Following this ground-breaking work, Engel and coworkers proposed TRPES on NaI.[43,44,116] While these studies have illustrated the utility of TRPES in observing wave-packet dynamics, Jouvet and coworkers have found a discrepancy between the theoretical prediction and the experimental result much later.[45] This was likely due to the fact that the ionization dipole moment function was assumed independent of internuclear distance. Charron and Suzer-Weiner have used an empirical form of the position-dependent dipole moment function to reproduce the experimental results.[46] Takatsuka, McKoy and their coworkers have attempted a more rigorous treatment of the underlying photoionization dynamics by including an accurate dipole moment function. They calculated photoionization amplitudes, C_{klm}, for each k-vector and (l, m) partial waves of the outgoing photoelectron as a function of internuclear distance from first principles, which yielded time-dependent PEDs and PADs in the ionization from the $^1\Sigma_u^+$

double minimum state of Na_2 [117–119] and the $^1\Sigma_0^+$ state of NaI.[120] The results clearly demonstrated the sensitivity of time-dependent PADs on vibronic wave-packet dynamics. Gerber and coworkers have employed femtosecond ZEKE spectroscopy to observe wave-packet motions in Na_3 in the B state.[121] Baumert and coworkers have studied vibrational wave-packet dynamics in the $2^1\Pi_g$ state of Na_2 [122] as mentioned in Sec. 2. Stolow and coworkers have used femtosecond ZEKE to probe vibrational wave-packet dynamics of I_2 in the $B(0_u^+)$ state.[123,124]

Syage has applied picosecond TRPES to reaction and solvation dynamics in hydrogen-bonded molecular clusters.[125,126] Phenol in the ammonia clusters was excited with 266 nm light, which induced a proton transfer to solvent molecules to form $PhO^- - H^+(NH_3)_n$. Soep and coworkers studied the excited state double proton transfer reaction in the 7-azaindole dimer by comparing the one-color (1 + 1) photoelectron spectra obtained with 0.8 and 5.0 ps laser pulses.[127] Stolow and coworkers have applied femtosecond TRPES to excited state proton transfer in *o*-hydroxybenzaldehyde (OHBA), its deuterated analogue (ODBA), and 1-hydroxy-2-acetonaphthone (HAN).[128] The enol form exhibited decay from the Franck–Condon region within the pulse duration <50 fs, which has been attributed to enol-keto tautomerization. This decay showed no isotope effect, suggesting a small or zero barrier for the reaction. The same group has also studied photodissociation of the nitric oxide dimer by TRPES using pump and probe wavelengths of 210 and 287 nm.[129] Although there are three reaction pathways forming the products NO(B) + NO(X), NO(A) + NO(X), and NO(X) + NO(X), 287 nm light could ionize only NO in the A state, in addition to the dimer from the Franck–Condon region. The NO dimer disappeared from the Franck–Condon region within 300 fs, while NO($A^2\Sigma^+$) fragments appeared around 700 fs, from which they suggested a two-step dissociation mechanism.[129]

Neumark and coworkers have studied photodissociation dynamics of I_2^- on the $A'^2\Pi_{g,1/2}$ state by femtosecond TRPES.[130,131] The pump pulse at 780 nm prepared a wave-packet on the repulsive state surface and the subsequent dynamics was interrogated by photodetachment using 260 nm light. The time-dependent signal was observed in the vicinity of the atomic ionization signals of I^- to $I(^2P_{1/2})$ and $I(^2P_{3/2})$. The reaction was completed within 300 fs. The same group has studied the ground state dynamics of I_2^- by creating a vibrational wave-packet by resonant impulsive stimulated Raman scattering and stimulated emission pumping using pump and dump pulses.[132,133] The wave-packet motion was observed by TRPES, and a high quality potential energy curve of I_2^- was obtained up to the dissociation limit. A similar study on $I_2^-(Ar)_n$ (n = 6–20)[134,135] showed that dissociation of I_2^- is completed within 300 fs. At later times, geminate recombination, vibrational relaxation, and solvent evaporation occurred in $I_2^-(Ar)_n$ ($n > 12$) in the X and A states. In similar experiments on $I_2^-(CO_2)_n$ (n = 4–16),[136,137] solvent rearrangement was observed at short time delays. Recombination, vibrational relaxation, and solvent evaporation were found to be faster than in the case of Ar clusters. Resonant impulsive Raman scattering was also used to observe the ground state dynamics of these clusters.[138]

In similar experiments on I_3^-,[139] dissociation occurred within several hundred femtoseconds yielding I_2^- in highly vibrationally excited states of $\langle v \rangle = 67$. Coherent vibrational wave-packet motion with a time period of 550 fs dephased in 4 ps, then rephased at 45 and 90.5 ps on the anharmonic vibrational potential curve of I_2^-. The gas-phase dissociation dynamics were found to be much different from those in solution. Charge transfer to solvent (CTTS) dynamics were studied for I^- solvated with Xe, H_2O, NH_3, CH_3OH.[140–143]

Zewail and coworkers have recently reported TRPES on mass-selected anions of molecular oxygen.[144]

4.3. *Photoelectron-Photoion Coincidence Detection*

Photoelectron-photoion coincidence techniques[145,146] may be used in conjunction with TRPES for several reasons. First of all, the coincidence method helps in disentangling photoelectron signals arising from ionization of a mixed ensemble of chemical species. If ionization is non-dissociative, each observed electron signal can be sorted out for different ion masses detected simultaneously to extract photoelectron spectra for different chemical species. This feature is particularly useful for studying neutral clusters where size selection prior to TRPES is complicated, although not impossible (see for example, NeNePo[40,147–154]). Radloff and coworkers have applied the method to explore excited state dynamics in benzene,[155] ammonia,[156–158] toluene[159] and their clusters. The second advantage of the coincidence method is its ability to discriminate between the mass signals for different MPI schemes. As an example, Fig. 4(a) shows time-resolved ion yield profiles in a femtosecond pump-probe experiment on OClO by Stert *et al.*[160] The molecule was excited to the $^2A_2$ state by a 298 nm 40 fs pump pulse and

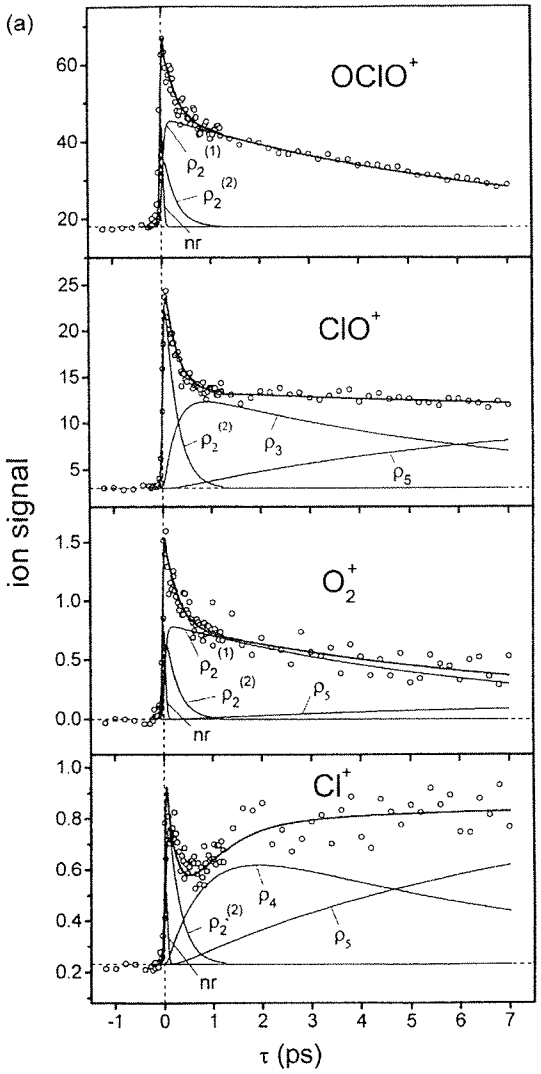

Fig. 4(a). Time-resolved ion yield profiles in a femtosecond pump-probe experiment on OClO by Stert *et al.*[160].

ionized by 265 nm 50 fs probe pulse. The photochemical reactions induced by 298 nm are

$$\begin{aligned} \mathrm{OClO}(\tilde{A}^2A_2) &\rightarrow \mathrm{ClO}(\tilde{X}^2\Pi) + \mathrm{O}(^3P) \\ &\rightarrow \mathrm{Cl}(^2P) + \mathrm{O}_2(^3\Sigma_g^-, {}^1\Delta_g, {}^1\Sigma_g^+). \end{aligned}$$

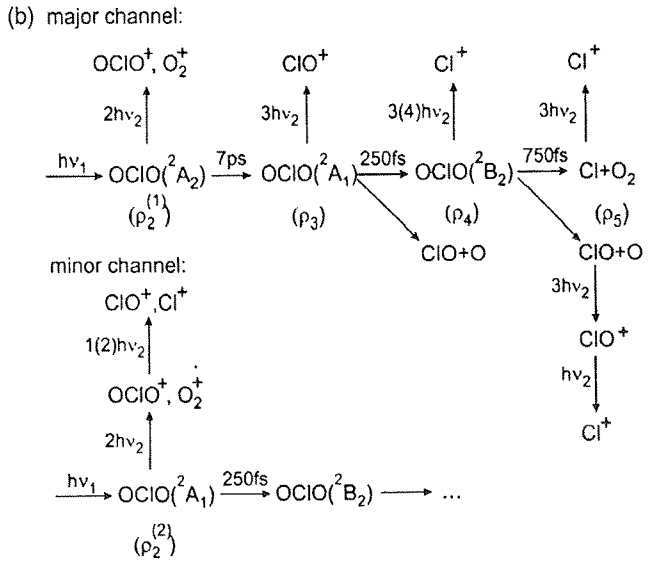

Fig. 4(b). Reaction scheme of OClO excited by the pump photon $\hbar\omega_1$ to the $^2A_2$ state (major channel) or $^2A_1$ state (minor channel). The different intermediate and final states are ionized by absorption of two to four probe photons $\hbar\omega_2$ and contribute to the signals as indicated in (a). Reproduced with permission from Ref. 160.

Since ionization by the probe pulse takes at least two photons from the $^2A_2$ state, the probe pulse induces other ionization processes as shown in Fig. 4(b). The photoelectron-photoion coincidence measurements are useful for disentangling this type of complication that is almost inevitable in any MPI probing of chemical reactions.

The level of sophistication or complexity is raised further, if one measures the kinetic energy of ions, the velocity distribution of ions, and the velocity distribution of electrons. For the latter two, imaging techniques are quite useful. The measurements of kinetic energies of ions are already advantageous for disentangling various processes observed simultaneously by MPI, since kinetic energies of ions are generally different for ionization of neutral fragment and dissociative ionization of a parent molecule.

Another important use of the coincidence detection technique is the observation of the MF-PAD, as mentioned in Sec. 2. When a molecule immediately dissociates upon ionization, the molecular axis at the instant of ionization is inferred from the recoil velocity of the fragments. Then, if one observes not only the mass, but also the recoil velocity direction of

the fragment, the molecular axis is defined in space. Simultaneous measurements of photoelectron recoil velocities establish vector correlations between the recoil velocities of the ions and the electron, i.e. MF-PADs.[52,53,56] Continetti and their coworkers have applied this method to UV photodissociaiton of negative ion clusters.[161,162] Hayden, Continetti and coworkers have combined this method with TRPES to explore photodissociation dynamics of NO_2 by measuring time resolved PADs.[38,39]

The challenge in the coincidence experiments is to perform measurements successfully with low count rates under the constraint that, in order to reject false coincidences, an electron signal must not be detected for every laser pulse.[146,161,163] In order to minimize the false coincidence rate, Radloff and coworkers suppressed the ionization events to be 0.3 per shot, from which a coincidence rate of 0.05 per laser shot was anticipated. False coincidences amounted to about 10%. On the other hand, uncorrelated measurements of photoelectrons described below have no limit for the number of electrons detected per a light pulse. Typically, the number of detected electrons is between 10 and 100 per pulse.

5. Time-Resolved Photoelectron Imaging

5.1. *Experimental Setup*

In the last decade, remarkable progress has been made in ultrafast laser technology, primarily due to the discovery of self-mode locking in Ti : sapphire crystals. Modern femtosecond laser technology is based on Ti : sapphire oscillators and amplifiers. A detailed description of laser techniques is beyond the scope of this article, and we briefly describe our experimental apparatus as an example of a standard femtosecond laser system.[36,37]

The system is divided into three parts, an oscillator, an amplifier, and optical parametric amplifiers (OPAs) (Fig. 5). In the past, when OPA was not used, a Ti : sapphire oscillator and an amplifier were tuned to a various wavelength from 700 to 1000 nm needed for experiments. However, this approach required tedious readjustment of optical devices inside an oscillator and an amplifier whenever the wavelength was changed. Such a procedure is no longer necessary with a modern system, since tunable light can be obtained at the final stage of a laser system using an OPA that enables straightforward scanning of the wavelength. (Note that the laser intensity obtainable with an OPA has a certain limit.) Therefore, the wavelength of an oscillator and an amplifier is often fixed at 800 nm. A Ti : sapphire

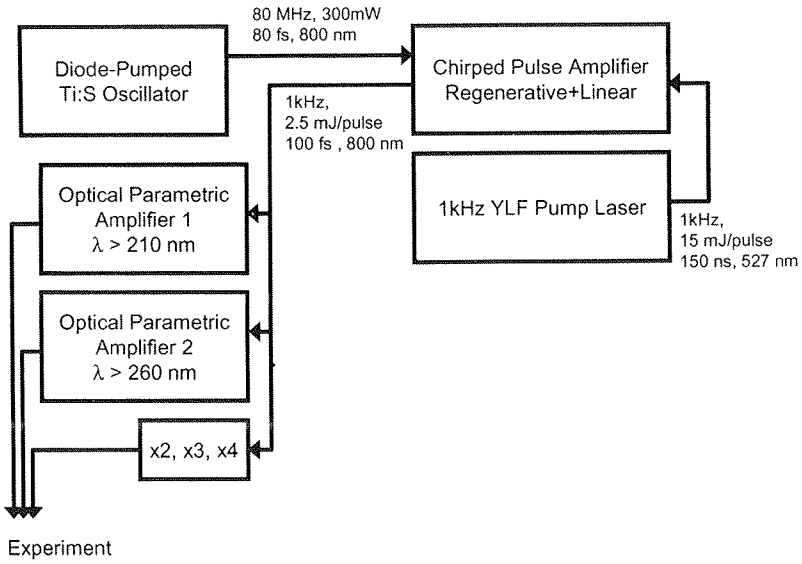

Fig. 5. Schematic diagram of a standard femtosecond laser system.

crystal in the oscillator is often pumped by a diode-pumped YVO_4 laser that is superior to a conventional Ar^+ ion laser because of lower noise and compactness, and less demands on electrical power and cooling water. The cavity of our oscillator uses specially coated mirrors in place of a prism pair to provide negative dispersion to the light pulse. The output from the oscillator, 80 MHz, 300 mW is introduced into a hybrid chirped pulse amplifier pumped by a Nd : YLF laser. Inside of the amplifier, the oscillator light pulse is first dispersively stretched to several hundred picoseconds by a grating to avoid any damage of optical components in the cavity, next it is amplified in a regenerative amplifier and a linear amplifier. The amplified pulse is finally recompressed by another grating to produce 1 kHz pulse train of $\sim$2.5 mJ pulse^{-1} light centered at $\sim$800 nm with a band width of 13 nm.

This amplified light is split into two equal intensity beams to pump two OPAs. Each OPA system has a computer controlled motor drive that adjusts the angles of crystals and a grating to maximize the OPA efficiency at each wavelength. Depending on the experiment, the second, the third, and the fourth harmonics of Ti : sapphire fundamental are also used. The cross-correlation of the pump and probe beams is typically 150–200 fs. The probe beam is optically delayed with respect to the pump beam using a hollow corner cube on a computer-controlled delay stage. The pump and

probe beams are directed into the molecular beam chamber either coaxially after merging them with a dielectric mirror or simply with a small angle (1°) without a mirror. Irises inserted into the optical paths of both the pump and probe beams are used to control the laser power entering the ionization chamber, and are adjusted so as to obtain the best contrast ratio for the two-color signal, as monitored from the photocurrent of a microchannel plate (MCP) detector.

A molecular beam chamber (Fig. 6) is a standard setup using differential pumping between a source chamber and an ionization chamber. A molecular beam is generated either by a pulsed valve driven by a piezoelectric crystal or a simple pinhole nozzle to generate a continuous stream of a sample gas. In either case, supersonic expansion cools down the rovibrational temperatures of molecules. We have switched from the former to the latter for higher stability that matches the stability of a laser system. A gas sample seeded in carrier gases of He, Ar, or molecular nitrogen is expanded at a stagnation pressure of *ca.* 500 torr from a pinhole 50 μm in diameter. The pressure in the source chamber is kept below 10^{-4} torr by means of a 2000 Ls^{-1} turbo molecular pump. The beam is skimmed and introduced into the ionization chamber where the background pressure (beam on) was *ca.* 10^{-7} torr, as maintained by 500 Ls^{-1} turbo molecular pump. Both turbo

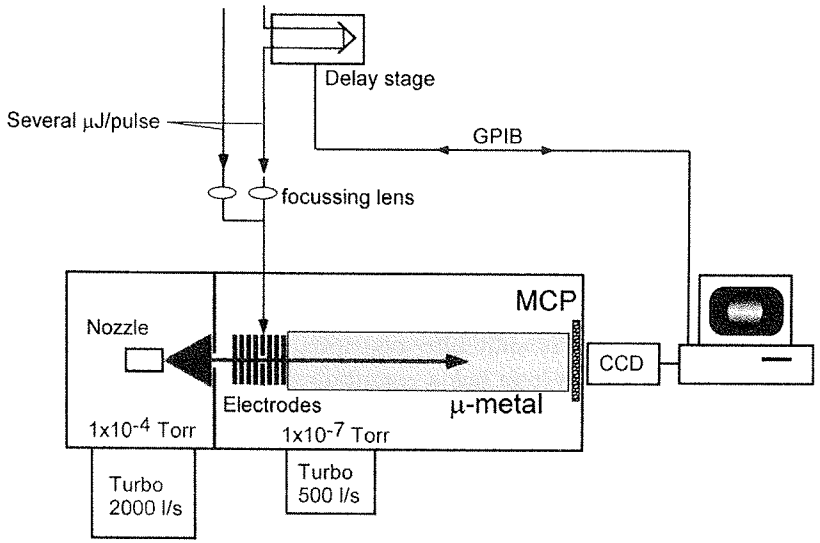

Fig. 6. Schematic diagram of a molecular beam photoelectron imaging apparatus.

molecular pumps are backed by a 37 m^3h^{-1} oil-free scroll pump and a liquid nitrogen trap placed in the fore line. Since a femtosecond laser pulse easily ionizes vapors of back-streamed pump oils, the oil-free vacuum system is important for good signal to noise ratio.

The pump and probe laser beams are crossed with a molecular beam in the static electric field in the velocity mapping mode.[30] A pump laser excites molecules in the beam to an electronically excited state, then a probe pulse ionizes the ensemble of molecules. The generated photoelectrons are accelerated parallel to the molecular beam and projected onto a position sensitive imaging detector. The detector consists of a 40 mm diameter dual MCP backed by a phosphor screen. Typically, P20 is used as a phosphor for its brightness and emission wavelength favorable for observation with a charge coupled device (CCD) camera. Light from the phosphor is coupled out of the vacuum chamber by means of a fiber bundle where it was recorded by a CCD camera with 512×512 pixels. The field-free region of the electron flight path was shielded with a μ-metal tube against stray magnetic fields.

An acceleration electrode is slightly different from that in a conventional Wiley–McLaren time-of-flight mass analyzer.[164] In usual TOF detectors, the acceleration electrodes have fine meshes to form completely flat electric fields, while a velocity mapping type of electrode forms an electrostatic immersion lens to deflect the electron trajectory slightly. The principle of velocity mapping has been discussed by Eppink and Parker.[30] This new type of electrodes focuses the electrons with the same velocity onto a single spot on the imaging detector, so the blurring of an image due to a finite size of an ionization region can be completely removed. A further improved design of electrodes that minimizes spherical and chromatic aberrations was presented by Wrede, Ashfold and coworkers more recently.[165,166]

5.2. *Image Transformation*

An observed image corresponds to a 2D projection of a 3D photoelectron scattering distribution. Therefore, computer tomography methods are applied to an observed photoelectron image to reconstruct the 3D distribution prior to a quantitative analysis. Reconstruction is possible from single projection data, when the 3D distribution has cylindrical symmetry and also the projection plane includes this symmetry axis.[23,167–169] In the pump-probe photoelectron imaging, cylindrical symmetry is ensured when the polarization of linearly polarized pump and probe light are aligned parallel to each other.

There are several types of transformation codes. The most widely used are an inverse Abel transformation[169,170] and a filtered back projection method.[166,171] Other reconstruction algorithms based on basis function expansions have also been reported.[172,173] An example of a transformation is shown in Fig. 7. When the signal to noise ratio is sufficiently high and the speed distribution is sharp, all of the codes provide the same result. On the other hand, when the noise is rather large, a part of the transformed image becomes unusable because of accumulated noise during the numerical transformation. In practice, this obvious noise appears in a narrow angular range and can be safely excluded in the analysis without losing any information.

Notice that the reconstruction provides the section of the 3D photoelectron scattering distribution, in which we see correlated speed and angular distribution of photoelectrons, in other word the doubly differential ionization cross section, directly. There is no complicated procedure of frame transformation between the laboratory frame and the center-of-mass frame, which is an important problem in conventional time-of-flight experiments of ions.

5.3. *Super-Excited States*

When ionization laser light is accidentally resonant with a transition from a neutral excited state to a super-excited state embedded in the ionization continuum, the PAD is strongly affected by this indirect ionization pathway. Figure 8 shows the PADs observed for one-color $(2+1)$ ionization of CO via the B state at 230 nm, in which PADs for different vibrational levels of CO^+ differ dramatically from each other.[174] Since the B state is a member of the Rydberg series converging to the ground state of CO^+, the ionization process is expected to be diagonal, dominated by the $\Delta v = 0$ transition. Hence, the appearance of the vibrational progression is unusual. In fact, a normal $\Delta v = 0$ propensity has been observed, when the probe laser wavelength was changed using a two-color $(2+1')$ REMPI scheme.[174] The super-excited states responsible for the anomaly are tentatively assigned

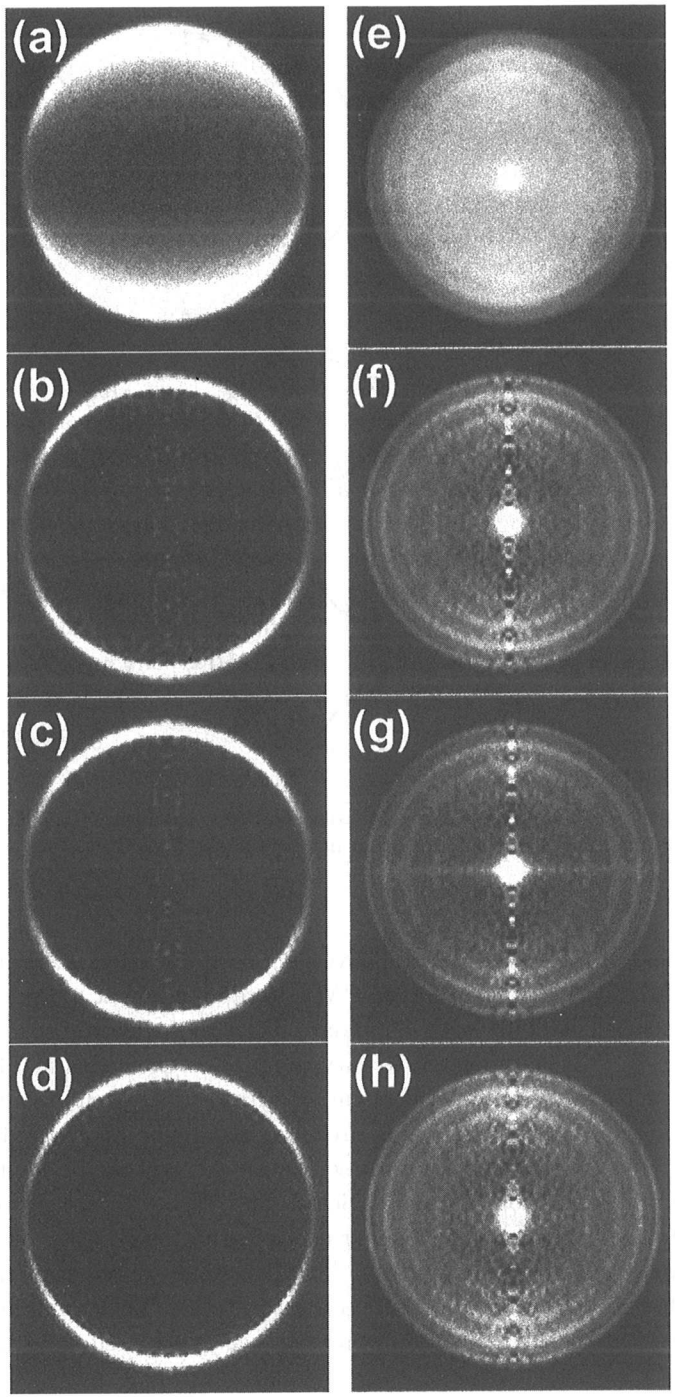

Fig. 7. Examples of transformation from the 2D projection data to the section of 3D scattering distribution. NO $(1+1')$ REMPI *via* A state $(v'=0)$: (a) raw data (2D projection), (b) an inverse Abel transformation, (c) a filtered back projection, and (d) an iterative fitting using basis functions.[172] Pyrazine $(1+1')$ REMPI *via* S_1 state $(v'=0)$: (e) raw data (2D projection), (f) an inverse Abel transformation, (g) a filtered back projection, and (h) an iterative fitting using basis functions.[172]

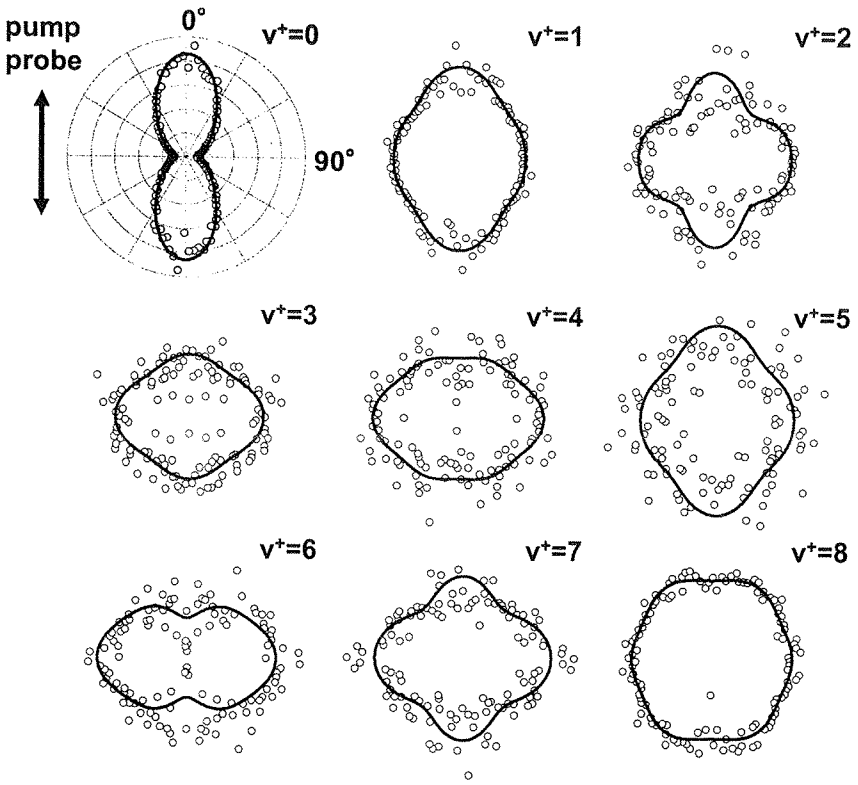

Fig. 8. Polar plots of PADs observed for one-color (2 + 1) ionization of CO *via* the B state at 230 nm. The vibrational quantum numbers of the final CO^+ state are referred to by v^+.

to members of a Rydberg series converging to the excited electronic state $A(^2\Pi)$ of the cation. The observed PADs were in excellent agreement with those measured carefully with a standard TOF photoelectron spectrometer by Sha *et al.*[175] It is important to vary the probe wavelength in TRPES in order to recognize resonance effects arising from super-excited states.

Although super-excited states are expected to be short-lived, pump-probe TRPES experiments on these states are scarce. In femtosecond multi-photon ionization of phenol, Schick and Weber found signatures of one-photon ionization out of a super-excited state reached by two-photon absorption from the ground state.[176,177] This super-excited state dephased into Rydberg states within a femtosecond time scale. This state, located at 9 eV, 0.5 eV above the ionization potential, was speculated to be a valence

type of excited state, differing in two electrons from the ground state: in order to reach the super-excited state in two-photon absorption, the first photon energy was resonant with transitions from S_0 to either S_1 or S_2, while the second photon energy was close to the electronic transition energy in the phenol cation, suggesting a stepwise two-electron promotion from the ground state electron configuration. It is quite interesting to explore the role of these states in ionization dynamics by using TRPEI in the future.

6. Time-Dependent Photoelectron Angular Distributions

6.1. *Rotational Wave-Packet Motion*

TRPES has demonstrated that the time-evolution of a non-stationary state appears as a variation in photoelectron kinetic energy distribution (PED). Another important observable in PES is the photoelectron angular distribution (PAD) that is the flux distribution of outgoing photoelectrons as a function of angle with respect to the ionization laser symmetry axis (the electric vector of linearly-polarized light or the k-vector of circularly polarized light). For one-photon ionization, the definite spin and parity of the ionizing photon define the PAD observable for a randomly oriented ensemble of targets.[178–180]

$$\frac{d\sigma}{d\Omega} = \frac{\sigma}{4\pi}[1 + \beta P_2(\cos\theta)]. \tag{1}$$

Here, $P_K(\cos\theta)$ is a Legendre polynomial. Similarly, for a two-photon process such as $(1 + 1')$ REMPI where the pump and probe laser polarizations are parallel to each other, the PAD is generally expressed by:

$$\frac{d\sigma}{d\Omega} = \frac{\sigma}{4\pi}[1 + \beta_2 P_2(\cos\theta) + \beta_4 P_4(\cos\theta)]. \tag{2}$$

In more general cases with non-parallel polarization combinations, the cylindrical symmetry breaks down, which gives rise to an azimuthal angle dependence of the PAD.

In 1978, Berry and coworkers have performed $(1+1')$ time-resolved PAD measurements on the $Na(3s^2S_{1/2})$ atom (F = 1 and 2) via the $3p^2P_{3/2}$ state with four hyperfine levels (F = 0, 1, 2 and 3).[181] A nanosecond laser pulse created a non-stationary coherent superposition of these hyperfine states, and the PADs were measured for different pump-probe polarization angles and time delays. The results clearly exhibited the time-dependent angular momentum polarization induced by the pump pulse. Leuchs *et al.* have reported more precise PAD measurements on the same system to see

revival features, and they extracted the time-dependent β_4 parameter that varied at least with two of the expected beat frequencies for the $^2P_{3/2}$ superposition state[182] (Fig. 9). The observed time-dependence of PADs is due to precession of the electron orbital induced by the angular momentum coupling between the electron orbital motion and the nuclear spin.

In molecular cases, coherent excitation of the P($\Delta J = -1$), $Q(0)$, and $R(+1)$ branch lines creates a superposition of molecular rotational eigenstates, i.e. a rotational wave-packet. The constructive and destructive interferences between different J components create a time-dependent molecular axis alignment that revives with characteristic time periods determined by rotational constants. Zewail, Felker and their coworkers have utilized these revival features to determine the structure of large molecules, which is known as rotational coherence spectroscopy (RCS).[183–187] The rotational wave-packet can be created also in the liquid phase, however, molecular collisions with solvents quickly destroy its coherent motion.[188–196] Therefore, a rotational wave-packet in solution is only observable as a dephasing at a very early time: this dephasing is termed anisotropy decay. In molecular

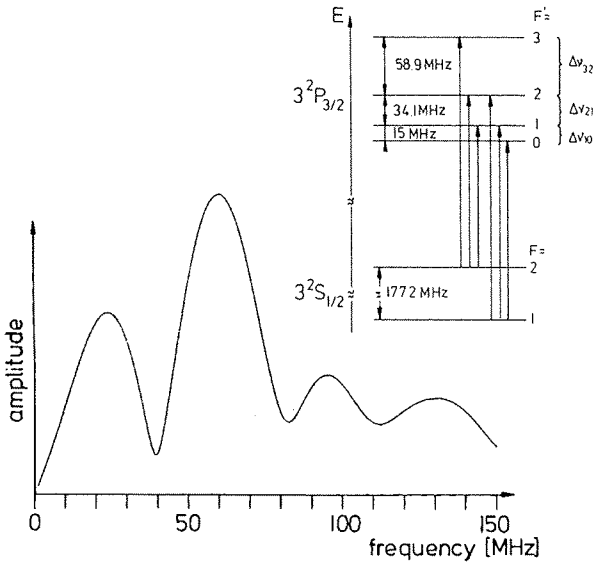

Fig. 9. Quantum beats observed in the time-dependent PAD in $(1+1')$ time-resolved PAD measurements of Na($3s^2S_{1/2}$) atom ($F = 1$ and 2) via the $3p^2P_{3/2}$ state with four hyperfine levels ($F = 0$, 1, 2 and 3). The figure shows the Fourier transform of the time-dependent anisotropy parameter β_4, the coefficient of the fourth-order Legendre polynomial. Reproduced with permission from Ref. 182.

photodissociation from an excited state with a finite lifetime, the anisotropy of the photofragment scattering distribution diminishes as a function of time due to a rotational dephasing, from which the lifetimes of excited states have been estimated.[197–199]

In the case of Na atom at a finite temperature, coherent excitation occurs from one hyperfine state in $3s\ ^2S_{1/2}$ to three hyperfine states in $3p\ ^2P_{3/2}$, while excitations starting from two different initial states of $F = 1$ and 2 in the $3s\ ^2S_{1/2}$ state are incoherently summed in the experimental observation.[181,182] Similar processes of thermal averaging are more extensive in the molecular case due to the finely spaced rotational level structure. The overall directional property of such an ensemble of molecules, in various j states and their superposition states, can be expressed by the distribution of the body-fixed frame with respect to the space-fixed frame defined by the Euler angles (θ, ϕ, χ). In the case of a symmetric top molecule, the molecular axis distribution is generally expressed by the following equation:

$$F(t,\theta,\phi) = \sum_{KQ} A_{KQ}(t) Y_{KQ}(\theta,\phi) \tag{3}$$

where the Y_{KQ} are spherical harmonics. In a cylindrically symmetric physical system such as one-photon excitation of randomly oriented molecules, the terms with $Q \neq 0$ are all zero:

$$F(t,\theta,\phi) = \sum_{K} A_{K0}(t) Y_{K0}(\theta,\phi) = \sum_{K} a_K(t) P_K(\cos\theta). \tag{4}$$

The highest rank is given by $K = 2n$, where n is the number of photons absorbed in the excitation step. As an example, Fig. 10 shows the alignment parameter A_{20}/A_{00} calculated for a one-photon transition of a symmetric top molecule. The J'' is the rotational angular momentum quantum number in the initial state, and each A_{20} value was calculated for a rotational wave-packet consisting of $J' = J''-1$, J'', and $J''+1$ components. The modulation of A_{20} is dependent on J''. When these modulations are summed over the initial J'' distribution at a finite temperature, the overall A_{20} of a molecular ensemble is obtained. This overall A_{20} exhibits sharp spikes at the revival times, since the rotational levels are regularly spaced ($2Bj$), and the full revival of all the wave-packets starting from different J'' simultaneously occur at $t = 2\pi/\omega_{\rm rot}$. The sharpness of the revival peak increases at higher temperatures, since a larger number of frequency components causes destructive interference except for the revival time. In the case of diatomic molecules with large rotational constants, only a few rotational levels are

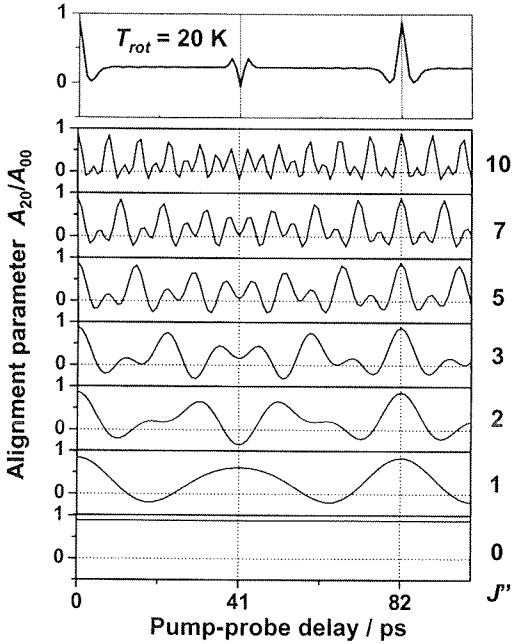

Fig. 10. Alignment parameter A_{20}/A_{00} calculated for a one-photon transition of a symmetric top molecule.

populated in a supersonic molecular beam, so their revival peaks become broad.

The PAD is expanded in spherical harmonics with weighting factors that vary with the time-dependent alignment (K = even) and/or orientation (K = odd) parameters.[200]

$$\frac{d\sigma}{d\Omega} = \frac{\sigma}{4\pi} \sum_{LQ} b_{LQ}(t) Y_{LQ}(\theta, \phi) \tag{5}$$

with

$$b_{LQ}(t) = \sum_{K} A_{K-Q}(t) P_{KLQ} \tag{6}$$

where L runs from zero up to $K_{\max} + 2$. The functions P_{KLQ} involve the dipole transition matrix elements and the phase shifts of the outgoing photoelectron partial waves. The most basic experiment in TRPEI is to obtain $A_{KQ}(t)$ from $b_{LQ}(t)$. Then, the photoionization stereodynamics may be elucidated from P_{KLQ}. Reid and coworkers attempted to extract $A_{KQ}(t)$ in the picosecond $(1+1)$ REMPI of p-difluorobenzene.[200,201] In ionization

with the parallel polarization combination of the pump and probe lasers, the PAD is expressed by:

$$\frac{d\sigma}{d\Omega} = \frac{\sigma}{4\pi} \sum_{L} \beta_L(t) P_L(\cos\theta) \tag{7}$$

with

$$\beta_L(t) = \sum_{K} A_{K0}(t) p_{KL}. \tag{8}$$

The example shown here is that of $(1+1')$ REMPI of NO via the $A(^2\Sigma^+)$ $3s$ Rydberg state, observed in our laboratory. Figure 11 shows the anisotropy parameters of the time-dependent PAD. The rotational temperature in the beam was estimated to be about 20 K, so the NO molecules were populated in the lowest few rotational levels in $^2\Pi_{1/2}$. The pump and probe laser beams were 226 and 285 nm, respectively, and their cross correlation was about 200 fs. The laser intensities were 7×10^8 W/cm^2 (pump)

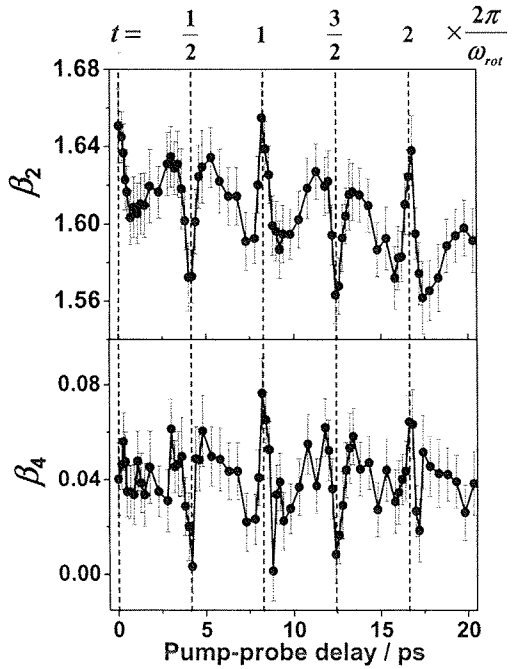

Fig. 11. Anisotropy parameters of the time-dependent PAD in $(1+1')$ REMPI of NO *via* the $A(^2\Sigma^+)3s$ Rydberg state.

and $10^{11}\,\mathrm{W/cm^2}$ (probe). Since the geometry of a Rydberg state is almost the same as that of a cation, the Franck–Condon propensity upon ionization is $\Delta v = 0$. The PED was essentially a single Gaussian function with a width determined by the energy resolution of PEI. Although variations of the anisotropy parameters against the time delay were only within 0.1, they were well reproducible and in excellent agreement with the expected time dependence of A_{20}. Slow variation of anisotropy parameters directly reflects the low rotational temperature in the molecular beam. More extensive measurements have revealed that anisotropy parameters vary with the probe laser wavelength and that the phase of modulation reverses at around $\lambda_{\mathrm{probe}} = 300\,\mathrm{nm}$. Althorpe and Seideman have simulated time-dependent PADs for different laser intensity regimes from 10^9 to $10^{13}\,\mathrm{W\,cm^{-2}}$ for $(1+1')$ REMPI of NO($X^2\Pi$) via $A(^2\Sigma^+)$ state.[202]

The advantage of using PAD measurements for detecting rotational wave-packet motion (or quantum beats) is that calibrations of the signal intensity for fluctuation of laser powers and beam walk-off are not necessary. The angular anisotropy determined from each PAD is highly reliable because all scattering angles are observed simultaneously, and is invariant to the total signal intensity fluctuation.

The signature of the rotational wave-packet could not be detected in the total ionization current of NO (NO^+ nor e^- signal). Indeed, as far as we know, observation of the rotational coherence in a total ionization signal in $(1+1')$ REMPI is limited to the case of *p*-cyclohexylaniline by Rien, Brutschy and coworkers.[203] Rien *et al.* carefully stated that the probing step leads either directly to the ionization continuum or into molecular Rydberg states that subsequently ionize.[203]

A one-photon transition with linearly polarized light creates a time-dependent alignment expressed by $A_{20}(t)$ in the neutral excited state, but when A_{20} becomes zero, the ensemble of molecules is seen as an isotropic target by a probe laser beam. Comparing the PADs expected for one-photon ionization of the isotropic ensemble (Eq. (1)) and of the polarized ensemble (Eq. (2)), it is clear that the highest rank anisotropy in $(1+1')$ REMPI, β_4, is most sensitive to the time-dependent molecular axis alignment. More clearly, Eq. (2) may be expressed by:

$$\begin{aligned}\frac{d\sigma}{d\Omega} &= \frac{\sigma}{4\pi}[1+b_2P_2(\cos\theta)] + \frac{\sigma'}{4\pi}\frac{A_{20}(t)}{A_{00}(t)}[1+b_2'P_2(\cos\theta)+b_4'P_4(\cos\theta)] \\ &= \frac{\sigma}{4\pi}[(1+g(t)) + (b_2+b_2'g(t))P_2(\cos\theta) + b_4'g(t)P_4(\cos\theta)] \qquad (9)\end{aligned}$$

where

$$g(t) = \frac{\sigma'}{\sigma}\frac{A_{20}(t)}{A_{00}(t)}.$$

In the above expression, σ' reflects the difference of the ionization transition dipole moment magnitudes for different axes in the molecular frame: in the case of NO, it is parallel or perpendicular to the molecular axis. When the transition dipole moments for ionization along the different axes in the molecular frame are similar in magnitude, $g(t)$ becomes very small, making it difficult to observe a rotational wave-packet motion in the total ionization current that is proportional to $1+g(t)$. The difficulty of observing rotational revival features in the total ionization signal has been addressed by Felker and Zewail who derived total ionization intensities in $(1+1')$ REMPI.[186,187] They speculated that the isotropic part of the tensor dominates over the anisotropic one, which reduces the dependence of $I(t)$ on the rotational anisotropy. This is exactly the case of small σ'/σ. Even in such a case, PADs should reflect the rotational wave-packet motion.

6.2. *Electronic Dephasing*

The photoelectron scattering distribution observed by PEI is essentially a doubly differential ionization cross section:

$$\frac{d^2\sigma}{dvd\Omega} = \frac{\sigma}{4\pi}P(v,t)\left[\sum_L \beta_L(v,t)P_L(\cos\theta)\right]. \qquad (10)$$

When the dephasing occurs from the initial (i) to the final (f) electronic state, the PAD may be decomposed into two contributions as follows:

$$\frac{d^2\sigma}{dvd\Omega} = \frac{\sigma}{4\pi}\sum_L\left\{P_i(v,t)\beta_L^i(v,t) + P_f(v,t)\beta_L^f(v,t)\right\}P_L(\cos\theta). \qquad (11)$$

In many cases, the above formula will be simplified to:

$$\frac{d^2\sigma}{dvd\Omega} = \frac{\sigma}{4\pi}\sum_L\left\{C_i(t)f_i(v)\beta_L^i(t) + C_f(t)f_f(v)\beta_L^f(t)\right\}P_L(\cos\theta) \qquad (12)$$

where the $f_i(v)$ and $f_f(v)$ are normalized speed distribution functions. After this decomposition into the individual components, the angular anisotropy parameters, β_L^i and β_L^f primarily reflect the rotational wave-packet motions. When the $P(v,t)$ is transformed into an energy scale, the PED is obtained. Electronic dephasing can be most easily detected from the time-dependence

of $P(v,t)$ or $C(t)$ in the above equations. However, when $f_i(v)$ is indistinguishable from $f_f(v)$, the PAD becomes the only observable for probing electronic dephasing. In this section, first we examine the general features of TRPEI in probing electronic dephasing, then we discuss the case where the dephasing is only probed from the PAD.

Since the pioneering work by Frad, Lahmani, Tramer and Tric, the $S_1(^1B_{3u})$ state of pyrazine has been the best-known example of an intermediate case in molecular radiationless transition theory.[204,205] It was predicted[206,207] that coherent excitation of an intermediate case molecule should exhibit a bi-exponential fluorescence decay, where the fast decay is due to the ultrafast dephasing of the optically prepared singlet state into a mixed singlet-triplet state and the slow decay is the depopulation of this mixed state. The bi-exponential fluorescence decay of S_1 pyrazine was extensively studied in the 1980s, and a debate ensued as to whether the fast component experimentally observed was due to the predicted dephasing or Rayleigh–Raman scattering. Picosecond laser spectroscopy was employed to confirm a finite fluorescence lifetime ($\tau \sim 110$ ps) longer than the laser pulse duration, proving that the fast component is fluorescence quenched by dephasing.[208–213] Consistency was also confirmed with high-resolution molecular eigenstate spectroscopy pioneered by Kommandeur, Meerts and coworkers.[214,215] However, these studies only observed the singlet character of the non-stationary state, and the dynamics in the triplet manifold remained to be examined. This classic problem was revisited by femtosecond TRPEI to shed light on the dark triplet manifold.

Figure 12 shows a series of photoelectron images observed by $(1+1')$ REMPI using 324 nm pump and 200 nm probe light at different time delays. All of the images were already Abel-transformed, so these correspond to the 2D sections of the 3D photoelectron scattering distributions: pyrazine molecules are located in the middle of each image, and outgoing photoelectrons are visualized at the point proportional to their scattering velocity vectors. The images observed at short time delays consist of a number of sharp rings. This structure disappears with a lifetime of 110 ps. Correspondingly, a low energy electron signal due to ionization from the triplet manifold grows in the inner part of the image: the triplet levels isoenergetic with the initially photoexcited singlet 0^0 level have large vibrational energies (4055 cm^{-1} in the case of T_1), and the Franck–Condon overlap favors ionization to highly vibrationally excited states in the cation. The sharp rings are transitions to overtone and combination levels of totally symmetric vibrational modes in the cation,[216] and their intensity distribution

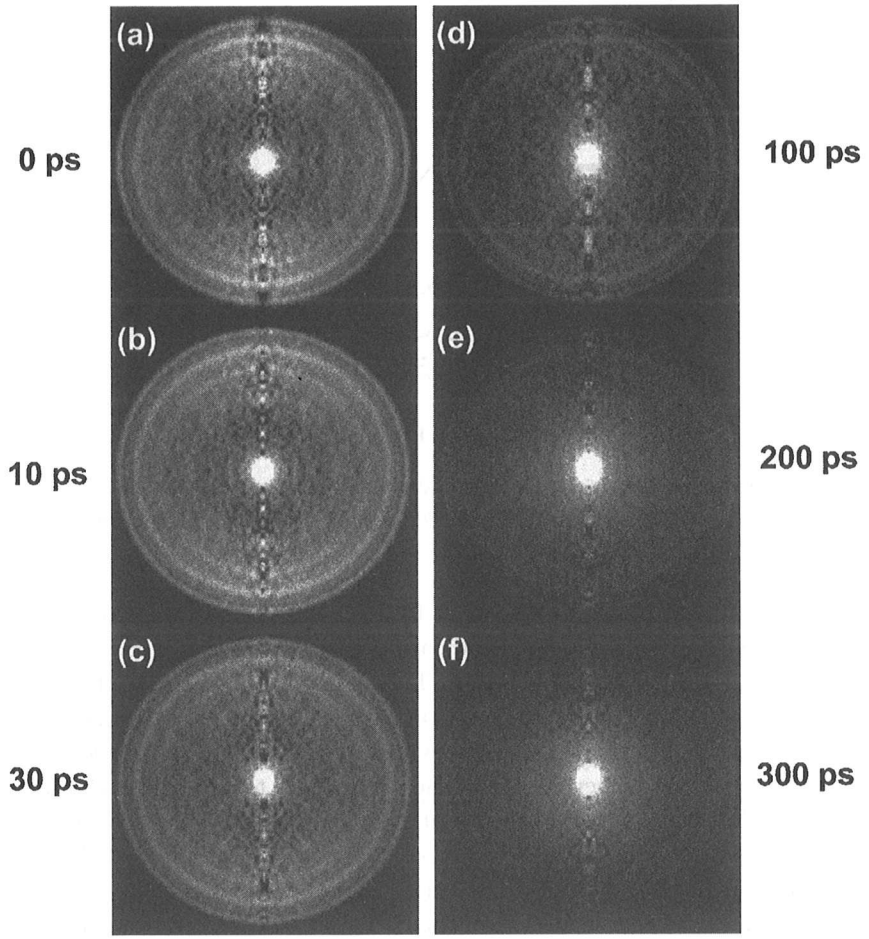

Fig. 12. Representative photoelectron images observed at different pump-probe time delays in $(1+1')$ REMPI of pyrazine. A 324 nm femtosecond pump pulse excited pyrazine to the S_1 0^0 level, and a time-delayed 200 nm femtosecond probe pulse ionized from the singlet and triplet states. The pump and probe laser polarizations are parallel to each other and in the vertical direction in the figure.

follows the Franck–Condon factors between the S_1 0^0 level and the cation. The pump and probe polarization directions are parallel to each other in the vertical direction in the figure. The angular anisotropy does exists, yet is rather weak ($\beta \sim 0.3$), reflecting the complex spatial structure of a π^* valence orbital from which an electron is ejected by the probe light.

As a conventional way of presentation, the PEDs were extracted from these images by integrating the angular part of the 2D photoelectron

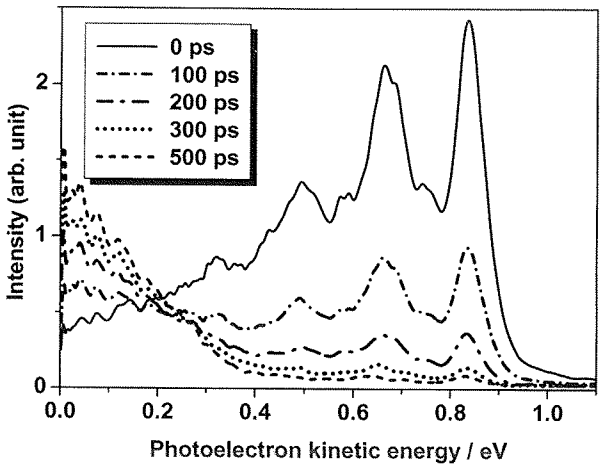

Fig. 13. PEDs extracted from the images shown in Fig. 12. All the spectra cross at the same energy (isosbestic point), indicating that the spectra consist of two components in dynamic equilibrium.

scattering distributions, as shown in Fig. 13. All the spectra cross at the same energy (isosbestic point), indicating that the spectra consist of two components in dynamic equilibrium. The ionization from the triplet manifold peaks at zero kinetic energy indicating that 200 nm is not a sufficiently short wavelength to ionize the entire vibrational wave-packet in the triplet manifold, making the sensitivity of the experiment to the triplet character relatively less than that for the singlet. Similarly, we have excited pyrazine to various vibronic levels in S_1 ($E_{vib} < 2000\,cm^{-1}$) and observed the photoelectron images. In all cases, the singlet signal decayed without changing its structure, meaning that IVR in the S_1 manifold does not occur prior to electronic dephasing due to the lack of sufficient vibrational state density. The same result has been obtained for deuterated pyrazine.

Smalley, Johnson and their coworkers have observed ionization from the triplet manifold in nanosecond $(1+1')$ REMPI.[217,218] Figure 14 shows the $(1+1')$ PED spectrum measured by Johnson and coworkers using nanosecond pump and probe light of 324 and *ca.* 200 nm, respectively.[218] The nanosecond result is in excellent agreement with TRPEI result at a long time delay (>300 ps). The results are also in qualitative agreement with the nanosecond PFI-ZEKE spectrum,[219] although ZEKE showed apparently smaller ionization signal from the triplet manifold, presumably due to the non-radiative decay of highly vibrationally excited ZEKE states prior to PFI.

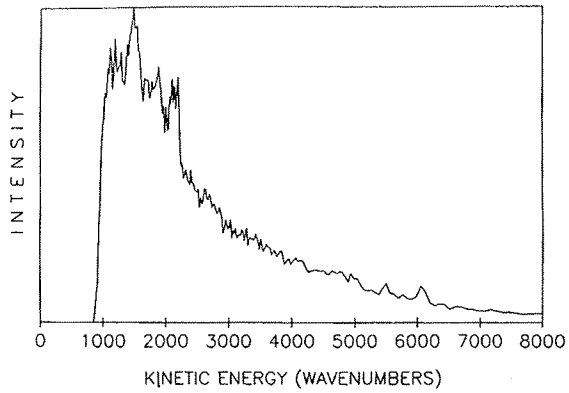

Fig. 14. $(1+1')$ PED spectrum measured by Johnson and coworkers using nanosecond pump and probe lasers at 324 and *ca.* 200 nm, respectively. Reproduced with permission from Ref. 218.

The angular anisotropy parameters in the singlet parts of the PADs are shown as a function of the pump-probe time delay in Fig. 15. The time dependence of the β_2 parameter is rather small, while the β_4 parameter shows a clear time dependence parallel to the calculated A_{20} parameter. Due to the selection rule of $\Delta J = 0, \pm 1$ ($\Delta K = 0$) in the initial $S_1 \leftarrow S_0$ pump step, there is only the J-coherence in the rotational wave-packet.

An interesting and somewhat complicated situation in pyrazine is that each zero-order rotational state in S_1 is coupled to tens of triplet vibronic states. How do such vibronic interactions affect the rotational wave-packets? To explore this problem, we employed $(1+2')$ REMPI as it is more sensitive to the rotational wave-packet motion both in the singlet and triplet manifolds. Two-photon ionization from the S_1 0^0 level *via* the $3s/3p$ Rydberg states was observed at the probe wavelength of 401 nm.[34,35,37] A series of observed photoelectron images is shown in Fig. 16. The strong anisotropy in the PADs is due to atomic-like electron orbitals in the intermediate Rydberg states. There are three major rings with different radii corresponding to PKEs of 40, 100 and 640 meV. Unlike in the $(1+1')$ REMPI case, these rings are *not* due to the vibrational structure in the cation but due to three different Rydberg intermediate states: the PKE for one-photon ionization *via* the Rydberg state is given by:

$$PKE = T(Rydberg) + \hbar\omega_2 - IP = \hbar\omega_2 - \frac{R}{(n-\delta)^2} \qquad (13)$$

where $\hbar\omega_2$ is the photon energy of the ionizing light. Appearance of only a single ring in the ionization from each Rydberg state is due to the

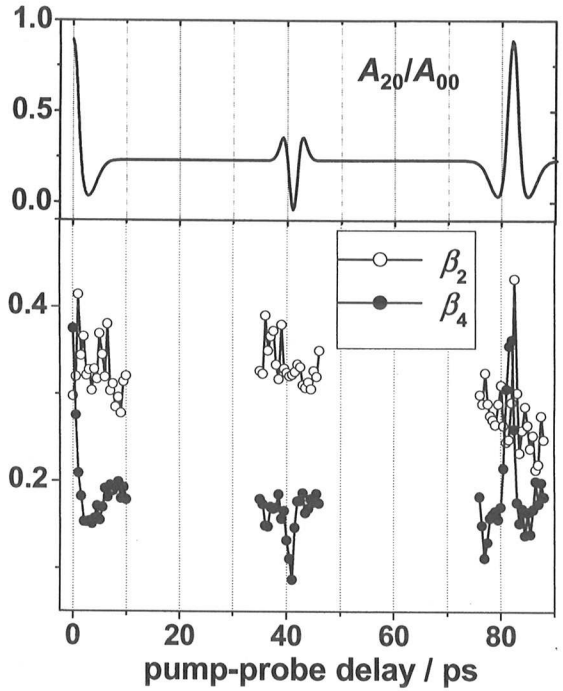

Fig. 15. Angular anisotropy parameters determined for the PAD in ionization from the singlet state.

vibrational selection rule $\Delta v = 0$. As Eq. (13) shows, the term value (the energy of the zero vibrational level) of a Rydberg state is readily obtained from the PKE.

According to Bethe[220] and Cooper and Zare[221] the anisotropy parameter associated with ionization of a one-electron atom is given by

$$\beta = \frac{l(l-1)r_{l-1}^2 + (l+1)(l+2)r_{l+1}^2 - 6l(l+1)r_{l+1}r_{l-1}\cos(\eta_{l+1} - \eta_{l-1})}{(2l+1)[lr_{l-1}^2 + (l+1)r_{l+1}^2]} \tag{14}$$

where $r_{l\pm1}$ are the transition dipole matrix elements for the $l \pm 1$ components of outgoing photoelectron wavefunctions, and $\eta_{l\pm1}$ denote the phases of these waves. For an s-electron, $l = 0$, the outgoing photoelectron is a pure p-wave, yielding $\beta = 2$. For other initial electron orbital angular momentum states, the magnitude of the anisotropy parameter is reduced as a result of interference between the two outgoing partial waves that are now possible (through the $\Delta\ell = \pm1$ electric dipole selection rule). Although

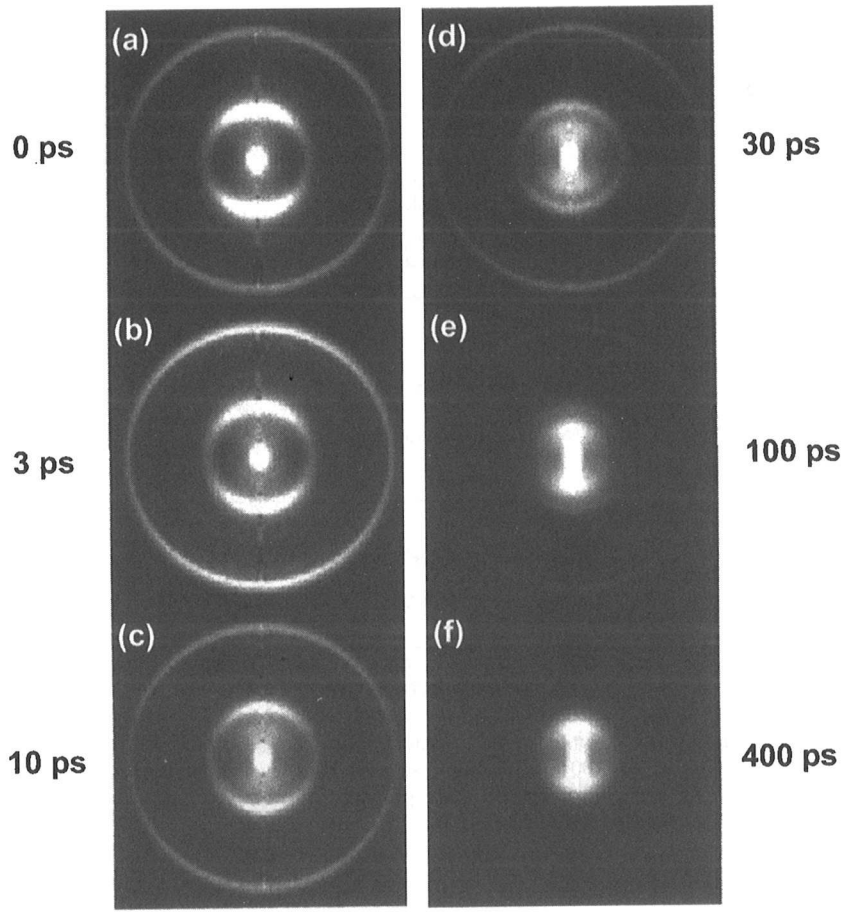

Fig. 16. Photoelectron images observed in the femtosecond $(1 + 1' + 1')$ REMPI of pyrazine. The pump laser at 324 nm excited pyrazine to the S_1 0° level, and the time-delayed probe laser pulse at 401 nm ionized the excited state by two-photon transition *via* the $3s/3p$ Rydberg states. The assignments of the rings are discussed in the text.

a rotational wave-packet affects the anisotropy parameter in the ionization of a molecule, the anisotropy parameters were found to be still useful in discriminating between the s and p molecular Rydberg states.[37] From the observed anisotropy and term values, the three rings were assigned to ionizations from S_1 via the singlet $3p$ and the singlet $3s$ state and ionization from T_1 *via* the triplet $3s$ state, in the decreasing order of PKE.

When the intensity and the angular anisotropy of these three photoelectron signals were examined, all of them exhibited clear revival features

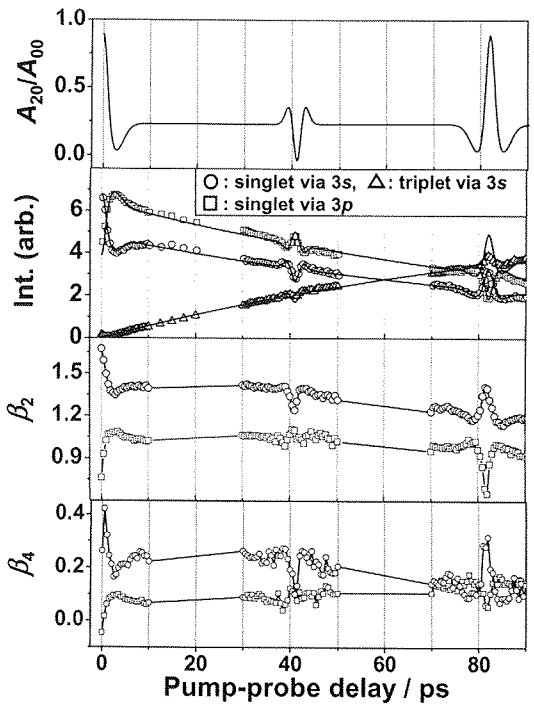

Fig. 17. Photoelectron intensity and angular anisotropy observed for three components with PKEs of 40, 100 and 640 meV seen in Fig. 16. For comparison, A_{20}/A_{00} was calculated for pyrazine in the S_1 state prepared by photoexcitation from S_0 at a rotational temperature of 20 K. Adopted from Ref. 36.

in the singlet and triplet states (Fig. 17). Since the Rydberg state is only used as a resonant state for femtosecond two-photon ionization from S_1, no rotational dynamics in the Rydberg state affects the signals: the time dependence originates from the rotational wave-packet motion in the S_1 and the T_1 states. From the initial rise and decay of the partial ionization signal intensity in $t < 3$ ps, it is concluded that the transition dipole for $3s \leftarrow S_1$ is parallel to that of $S_1 \leftarrow S_0$ while the $3p \leftarrow S_1$ transition dipole is perpendicular to the $S_1 \leftarrow S_0$ dipole. The ionization signals from the singlet characters *via* the $3s$ and $3p$ singlet states exhibit opposite phase of modulation, indicating that the two transition dipoles of $3s \leftarrow S_1$ and $3p \leftarrow S_1$ are perpendicular to each other. Since the $S_1 \leftarrow S_0$ dipole is along the figure axis of this near oblate top (the out-of-plane x axis), the $3s \leftarrow S_1$ and $3p \leftarrow S_1$ dipoles are parallel and perpendicular to the figure axis. Obviously, a one-photon transition from π^* to $3p$ is forbidden between

orbitals of ungrade symmetry, and the transition is vibronically induced by excitation of the mode 11 (b_{3u}).

For analyzing the rotational wave-packet dynamics, model calculations were performed. The triplet vibronic level structure was generated randomly with a variable level density ρ, and the rotational level structures of an oblate top were added to each of these vibronic levels to form the entire dark state manifold. A Hamiltonian matrix including each zero-order singlet rovibronic state and many triplet states was constructed by assuming a constant spin-orbit coupling strength V. The singlet-triplet angular momentum coupling was explicitly taken into account in the off-diagonal elements: one molecular rotational state in the singlet is coupled to six rotational states in a triplet vibronic state under the constraint of $\Delta J = 0$. The A, B, and C rotational constants in the singlet state, 6.1035, 6.0813 and 3.0477 GHz, respectively were taken from the literature.[222] By diagonalizing the Hamiltonian matrix, the ensemble of mixed singlet-triplet states was calculated for each zero-order singlet rotational level. The time-evolution after the coherent excitation of the P, Q, and R branch lines at the rotational temperature of 20 K in the molecular beam was computed. The two parameters ρ and V were adjusted to reproduce the observed electronic dephasing time of S_1 pyrazine.

As known from the 1980s, the (pseudo)exponential decay of the bright state is observed when all the eigenstates are considered without exception. When the states with small amplitudes of the singlet character (*grass*) are intentionally neglected, the decay profile becomes non-exponential. We also confirmed that, only when all the molecular eigenstates are taken into account, the rotational wave-packet in the singlet manifold fully revives. Model calculations were performed without truncating the eigenvectors with small amplitudes. The revival time in the singlet state was unaffected by the coupling with the triplet state, and the revival time in the triplet manifold was essentially the same as that of the singlet and invariant to the rotational constants in the triplet state. This is due to the fact that the photoexcitation of the triplet states is limited in the vicinity of the zero-order singlet state with the small coupling strength, and the quantum beat frequencies are primarily determined by the singlet rotational constants. The differences in the height and width of rotational revival peaks between the singlet and triplet are speculated to be due to the J-dependent $S_1 - S_0$ or $T_1 - S_0$ couplings that are not included in the model yet. A more complete analysis is in progress in our laboratory.

When $f_i(v)$ and $f_f(v)$ are indistinguishable, the PAD measurement becomes a unique way of detecting the electronic dephasing. An example from our own studies is internal conversion between the Rydberg states of the pyrazine molecule. Excited electronic states of pyrazine exhibit large geometrical changes along the $6a(a_g)$ vibrational coordinate[106–109] which leads to conical intersections between S_2 and S_1 as well as between the first excited state, D_1 (π^{-1}), and the ground state, $D_0(n^{-1})$, of the cation. Since all the Rydberg series converging to a cationic electronic state have essentially the same vibrational potential as the cation, Rydberg states with the same principal and angular momentum quantum numbers with different ion cores of n^{-1} and π^{-1} undergo conical intersections. The lifetime for internal conversion from $D_1(\pi^{-1})$ to $D_0(n^{-1})$ has been estimated to be 30 fs,[223] which is quite similar to the case of $S_2 - S_1$ internal conversion. Thus, if the $3s(\pi^{-1})$ Rydberg state is optically prepared, it may dephase to $3s(n^{-1})$ in 30 fs. We have performed $(2+1)$ one-color REMPI-PES with 100 fs laser pulse via the $3s(\pi^{-1})$ state and examined whether the ionization from the $3s(n^{-1})$ state was observed.[37]

As Eq. (12) shows, two Rydberg states with the same n and l quantum numbers in the series converging to the $D_1(\pi^{-1})$ and $D_0(n^{-1})$ ionic states exhibit only a small difference in their PKEs due to extremely similar quantum defects. The PKE in the ionization from the $3s(\pi^{-1})$ to the D_1 state should be 60 meV lower than that in the ionization from the $3s(n^{-1})$ to $D_0(n^{-1})$. However, this shift could not be resolved clearly with the energy resolution of our photoelectron imaging apparatus.[37] Alternatively, electronic dephasing was examined through the PADs. When the same laser pulse prepares the $3s$ state and ionizes out of this state, the molecular rotation can be ignored within the laser pulse duration (100 fs) and the PAD is determined by photoionization dynamical parameters with molecular alignment parameter at $t = 0$. The alignment parameter is estimated from the two-photon transition tensor between the $3s(\pi^{-1})(^1B_{1g})$ state and the ground state mediated by B_{2u} or B_{3u} virtual states:

$$\langle B_{1g}|x|B_{2u}\rangle\langle B_{2u}|y|A_g\rangle \quad \text{or} \quad \langle B_{1g}|y|B_{3u}\rangle\langle B_{3u}|x|A_g\rangle.$$

From group theoretical arguments, the molecular axis possesses primarily an alignment $\cos^2\theta\sin^2\theta$ with respect to the laser polarization. The dynamical parameters for one-photon ionization from the $3s(n^{-1})$ state were obtained by the PAD measurements in $(2+1)$ ionization *via* the $3s(n^{-1})$ state and $(1+1'+1')$ ionization *via* S_1 and $3s(n^{-1})$. The former ionization occurred from the alignment approximately proportional to $\sin^4\theta$, while the latter took place from an alignment proportional to $\cos^4\theta$. From these parameters, the PAD anticipated for ionization from the $3s(n^{-1})$ with the $\cos^2\theta\sin^2\theta$ molecular axis alignment was calculated. The calculated and observed PADs were found to be different, suggesting that the internal conversion from the $3s(\pi^{-1})$ to the $3s(n^{-1})$ state is not completed within the laser pulse duration.[37]

Seideman has simulated time-dependent PADs in the photoionization of octatetraene that undergoes ultrafast electronic dephasing from $S_2(1B_u)$ to $S_1(2A_g)$. The PAD in the lab frame considerably changes upon dephasing, even though that of the MF-PAD is more dramatic.[224,225] In the formulation by Takatsuka, McKoy and their coworkers, the photoionization amplitude for a molecule fixed in space has been rigorously calculated. In more recent work, they included molecular rotational motion classically, because of the computational difficulty in treating this motion fully quantum-mechanically.[119]

6.3. *Photoionization Stereodynamics*

When molecules are definitely oriented in space, the PAD can be expressed by:[226,227]

$$\frac{d\sigma}{d\Omega} = \sum_{K=0}^{2l_{\max}} \alpha_{KM} Y_{KM}(\theta,\phi), \tag{15}$$

where θ and ϕ are measured from the z axis in the molecular frame, and $l_{\max}$ is the largest orbital angular momentum component of the outgoing photoelectron. The MF-PAD is by far more structured than the PAD observable in the lab frame, as the highest rank allowed for the latter is only $K = 2n$ for n-photon ionization of a randomly oriented target. The MF-PAD provides detailed information on the transition dipole moments and phase shifts for each partial wave of an outgoing electron. For extracting similarly detailed dynamical parameters from the PAD in the lab frame, Zare and coworkers have observed the PAD in nanosecond $(1+1')$ REMPI of NO by defining the initial and the final rotational quantum number, for various experimental geometries, using linear and circularly polarized light.[228–234] The rotational resolution in PES was used to resolve the partial wave compositions of photoelectrons through the angular momentum conservation law between the rotational quantum number in NO^+ and the photoelectron orbital angular momentum.[234–238]

In TRPES experiments, extraction of photoionization dynamical parameters has not been achieved yet. More quantitative results have been reported so far. An example shown here is three-photon ionization of pyrazine via the $3s(n^{-1})\ ^1A_g$ Rydberg state. Since the $3s(n^{-1})$ state decays in 300 fs,[239] no rotational wave-packet motion can be created in this electronic state. Instead a wave-packet was launched on the $S_1(n,\pi^*)$ state followed by two-photon ionization via the $3s$ state. Since both the $S_1(^1B_{3u})$–$S_0(A_g)$ and $3s(A_g)$–$S_1(^1B_{3u})$ are parallel transitions of an oblate top, the molecular axis alignment was only weakly modulated around a $\cos^4\theta$ distribution. To achieve an extremely different alignment, non-resonant two-photon pumping to the $3s(n^{-1})$ state was also employed, for which nearly $\sin^4\theta$ alignment is anticipated. The PADs observed for $\cos^4\theta$ and $\sin^4\theta$ molecular axis alignments are shown in Fig. 18. The PADs are highly anisotropic and peaked along the laser polarization as expected from the dominant p-wave character of the outgoing electrons in ionization from the s state. The widths of the PADs point to the scattering of outgoing electrons by valence electrons, in particular, in the molecular plane. From the observed PADs, the geometrical parameters for calculating the PADs for other alignment were obtained. The PADs vary with the strength of molecular axis alignment, however, its magnitude is rather modest. Two speculative arguments are given to rationalize this observation. One is that

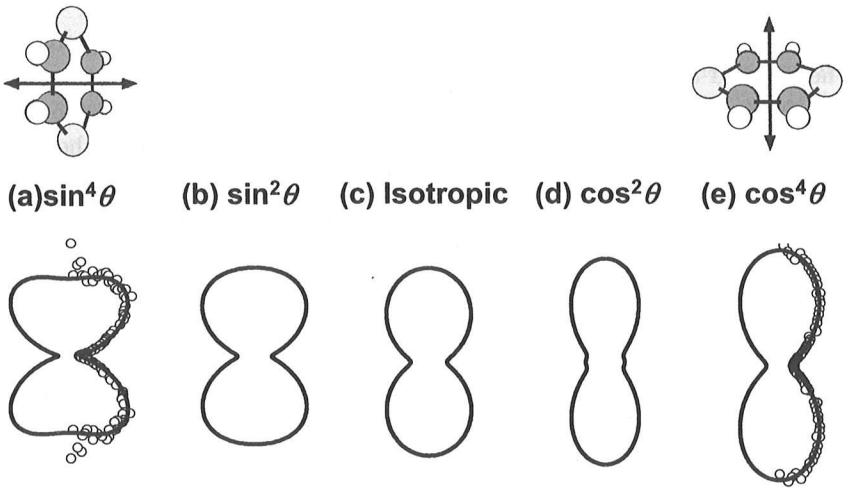

Fig. 18. PAD observed for (a) $\sin^4\theta$ and (e) $\cos^4\theta$ molecular axis distributions and calculated ones for other axis distributions of (b) $\sin^2\theta$, (c) isotropic and (d) $\cos^2\theta$.

the $3s$ Rydberg orbital is located reasonably well outside the ion core where the character of the outgoing partial wave may be weakly dependent on the molecular alignment. The other is that the strength of the axis alignment, when measured by FWHM, is not largely different for $\cos^2\theta$, and $\cos^4\theta$, note that the widths (FWHM) of the axis alignments in the $\cos^4\theta$ distribution, 65°, and $\cos^2\theta$ distribution, 90°, are not significantly different. Since a specific orbital angular momentum in the Rydberg state restricts the number of partial waves in the outgoing electron, the molecular frame PAD will not be highly structured. In this sense, the former argument is more likely to be applicable in this particular case of a Rydberg state. However, the latter argument should also be considered, since it limits the dependence of MF-PADs on the alignment created by multi-photon processes.

7. Outlook

Time-resolved photoelectron spectroscopy, particularly in the form of electron imaging, provides extremely rich information on the excited state dynamics of molecules and clusters. With the advent of non-linear optical technologies to generate femtosecond (and attosecond[21,240,241]) extreme ultraviolet laser pulses, further exciting experiments of femtochemistry and attophysics will be possible with TRPEI using short wavelength lasers. Observation of angular distributions for high-energy electrons requires further improvements in the imaging methods. At the moment, a CCD camera-based imaging method is advantageous for observing multiple electron hits per light pulse and its ease of use, while its time resolution is much poorer than that of electrical imagers such as delay line detectors. Further development of a camera system for obtaining superior time-resolution and faster readout clock rates ($\gg$30 frames/s) is highly desirable.

In view of the importance of photoionization/photodetachment studies of chemical reactions, accurate theoretical predictions of time-dependent PEDs and PADs for closer comparison with experimental results are highly desired. A detailed analysis of the photionization dynamics in the probing step is indispensable for extracting information on the reaction dynamics of interest from the observed results. At the moment, rigorous calculations are computationally demanding even for a diatomic molecule for a large number of ionization channels, so any effective approximations to facilitate the treatment of large polyatomic molecules will be extremely useful.

In order to approach the MF-PAD by observing the PAD in the laboratory frame, the molecular axis distribution must be narrowed down. As one

of the approaches, a moderate off-resonant intensity pulse (*ca.* 10^{12} W/cm) can be used for prealignment of a molecular ensemble in the ground electronic state. When pump and probe experiments are performed at the first full revival of the rotational wave-packet, the influences of the prealignment laser upon ionization process will be completely negligible.

Acknowledgments

Financial support from the Ministry of Education, Culture, Sports, Science and Technology of Japan is gratefully acknowledged. We thank Eckert Wrede, Marc Vrakking, and Hanna Reisler for kind offer of their transformation codes and Kees de Lange for careful reading of the manuscript.

References

1. M. I. Al-Joboury and D. W. Turner, *J. Chem. Phys.* **37**, 3007 (1962).
2. F. I. Vilesov, B. C. Kurbatov, A. N. Terenin, *Dokl. Akad. Nauk SSSR* 138 (1961).
3. T. Koopmans, *Physica* **1**, 104 (1933).
4. A. Azabo and N. S. Ostlund, *Modern Quantum Chemistry: Introduction to Advanced Electronic Structure Theory* (Dover, New York, 1996).
5. D. W. Turner, C. Baker, A. D. Baker and C. R. Brundle, *Molecular Photoelectron Spectroscopy: A Handbook of He 584 A Spectra* (Wiley Interscience, 1970).
6. J. H. D. Eland, *Photoelectron Spectroscopy* (Wiley-Halsted, 1974).
7. J. W. Rabalais, *Principles of Ultraviolet Photoelectron Spectroscopy* (Wiley-Interscience, New York, 1977).
8. J. Berkowitz, *Photoabsorption, Photoionization, and Photoelectron Spectroscopy* (Academic Press, 1979).
9. K. Kimura, S. Katsumata, Y. Achiba, T. Yamazaki and S. Iwata, *Handbook of HeI Photoelectron Spectra of Fundamental Organic Molecules* (Japan Scientific Societies Press, 1981).
10. S. R. Long, J. T. Meek and J. P. Reilly, *J. Chem. Phys.* **79**, 3026 (1983).
11. Y. Achiba, K. Sato, K. Shobatake and K. Kimura, *J. Chem. Phys.* **78**, 5474 (1983).
12. Y. Achiba, K. Sato, K. Shobatake and K. Kimura, *J. Chem. Phys.* **79**, 5213 (1983).
13. Y. Achiba, A. Hiraya and K. Kimura, *J. Chem. Phys.* **80**, 6047 (1984).
14. A. Hiraya, Y. Achiba, N. Mikami and K. Kimura, *J. Chem. Phys.* **82**, 1810 (1985).
15. T. Baumert, J. Helbing and G. Gerber, *Adv. Chem. Phys.* **101**, 47 (1997).
16. J. L. Knee, *High Resolution Laser Photoionization and Photoelectron Studies*, eds. I. Powis, T. Baer, C. Y. Ng (John Wiley, 1995).
17. C. C. Hayden, A. Stolow, *Photoionization and Photodetachment*, ed. C. Y. Ng (World Scientific, Singapore, 1999) p. 91.

18. T. Suzuki and B. J. Whitaker, *Int. Rev. Phys. Chem.* **20**, 313 (2001).
19. D. Neumark, *Ann. Rev. Phys. Chem.* **52**, 255 (2001).
20. T. Seideman, *Ann. Rev. Phys. Chem.* **53**, 41 (2002).
21. T. Brabec and F. Krausz, *Rev. Mod. Phys.* **72**, 545 (2000).
22. D. L. Ames, J. P. Maier, F. Watt and D. W. Turner, *Faraday Discuss.* 277 (1972).
23. H. Helm, N. Bjerre, M. J. Dyer, D. L. Huestis and M. Saeed, *Phys. Rev. Lett.* **70**, 3221 (1993).
24. M. Saeed, M. J. Dyer and H. Helm, *Phys. Rev.* **A49**, 1491 (1994).
25. C. Bordas, M. J. Dyer, T. A. Fairfield, M. Saeed and H. Helm, *J. Phys.* **IV4**, 647 (1994).
26. W. K. Kang, Y. S. Kim and K. H. Jung, *Chem. Phys. Lett.* **244**, 183 (1995).
27. C. Bordas, M. J. Dyer, T. Fairfield, H. Helm and K. C. Kulander, *Phys. Rev.* **A51**, 3726 (1995).
28. C. Bordas, F. Paulig, H. Helm and D. L. Huestis, *Rev. Sci. Instr.* **67**, 2257 (1996).
29. Y. J. Jung, Y. S. Kim, W. K. Kang and K. H. Jung, *J. Chem. Phys.* **107**, 7187 (1997).
30. A. Eppink and D. H. Parker, *Rev. Sci. Instr.* **68**, 3477 (1997).
31. C. Bordas and J. C. Pinare, *Phys. Rev.* **A57**, R681 (1998).
32. C. Bordas, *Phys. Rev.* **A58**, 400 (1998).
33. J. Winterhalter, D. Maier, J. Honerkamp, V. Schyja and H. Helm, *J. Chem. Phys.* **110**, 11187 (1999).
34. T. Suzuki, L. Wang and H. Kohguchi, *J. Chem. Phys.* **111**, 4859 (1999).
35. L. Wang, H. Kohguchi and T. Suzuki, *Faraday Discuss.* 37 (1999).
36. M. Tsubouchi, B. J. Whitaker, L. Wang, H. Kohguchi and T. Suzuki, *Phys. Rev. Lett.* **86**, 4500 (2001).
37. J. K. Song, M. Tsubouchi and T. Suzuki, *J. Chem. Phys.* **115**, 8810 (2001).
38. J. A. Davies, J. E. LeClaire, R. E. Continetti and C. C. Hayden, *J. Chem. Phys.* **111**, 1 (1999).
39. J. A. Davies, R. E. Continetti, D. W. Chandler and C. C. Hayden, *Phys. Rev. Lett.* **84**, 5983 (2000).
40. E. Schreiber, *Femtosecond Real-Time Spectroscopy of Small Molecules and Clusters*, Springer, Berlin Heidelberg, New York, 1998.
41. V. Engel and H. Metiu, *Chem. Phys. Lett.* **155**, 77 (1989).
42. V. Engel and H. Metiu, *J. Chem. Phys.* **90**, 6116 (1989).
43. C. Meier and V. Engel, *J. Chem. Phys.* **101**, 2673 (1994).
44. M. Braun, C. Meier and V. Engel, *J. Chem. Phys.* **105**, 530 (1996).
45. C. Jouvet, S. Martrenchard, D. Solgadi, C. Dedonderlardeux, M. Mons, G. Gregoire, I. Dimicoli, F. Piuzzi, J. P. Visticot, J. M. Mestdagh, P. Doliveira, P. Meynadier and M. Perdrix, *J. Phys. Chem.* **A101**, 2555 (1997).
46. E. Charron and A. Suzor-Weiner, *J. Chem. Phys.* **108**, 3922 (1998).
47. A. Assion, T. Baumert, V. Seyfried, V. Weiss, E. Wiedenmann and G. Gerber, *Z. Phys. D-At. Mol. Clusters* **36**, 265 (1996).

48. J. B. Hopkins, D. E. Powers, S. Mukamel and R. E. Smalley, *J. Chem. Phys.* **72**, 5049 (1980).
49. J. B. Hopkins, D. E. Powers and R. E. Smalley, *J. Chem. Phys.* **72**, 5039 (1980).
50. J. B. Hopkins, D. E. Powers and R. E. Smalley, *J. Chem. Phys.* **73**, 683 (1980).
51. S. Kaesdorf, G. Schonhense and U. Heinzmann, *Phys. Rev. Lett.* **54**, 885 (1985).
52. A. V. Golovin, *Opt. Spektrosk.* **71**, 933 (1991).
53. A. V. Golovin and P. G. Cheremnykh, *Instr. Exp. Tech.* **34**, 385 (1991).
54. A. V. Golovin, *J. Electron Spectrosc. Relat. Phenom.* **96**, 117 (1998).
55. E. Shigemasa, J. Adachi, M. Oura and A. Yagishita, *Phys. Rev. Lett.* **74**, 359 (1995).
56. P. A. Hatherly, J. Adachi, E. Shigemasa and A. Yagishita, *J. Phys. B-At. Mol. Opt. Phys.* **28**, 2643 (1995).
57. N. Watanabe, J. Adachi, K. Soejima, E. Shigemasa, A. Yagishita, N. G. Fominykh and N. A. Cherepkov, *Phys. Rev. Lett.* **78**, 4910 (1997).
58. E. Shigemasa, J. Adachi, K. Soejima, N. Watanabe, A. Yagishita and N. A. Cherepkov, *Phys. Rev. Lett.* **80**, 1622 (1998).
59. K. Ito, J. Adachi, Y. Hikosaka, S. Motoki, K. Soejima, A. Yagishita, G. Raseev and N. A. Cherepkov, *Phys. Rev. Lett.* **85**, 46 (2000).
60. S. Motoki, J. Adachi, Y. Hikosaka, K. Ito, M. Sano, K. Soejima, A. Yagishita, G. Raseev and N. A. Cherepkov, *J. Phys. B-At. Mol. Opt. Phys.* **22**, 4193 (2000).
61. N. A. Cherepkov, G. Raseev, J. Adachi, Y. Hikosaka, K. Ito, S. Motoki, M. Sano, K. Soejima and A. Yagishita, *J. Phys. B-At. Mol. Opt. Phys.* **33**, 4213 (2000).
62. F. Heiser, O. Gessner, U. Hergenhahn, J. Viefhaus, K. Wieliczek, N. Saito and U. Becker, *J. Electron Spectrosc. Relat. Phenom.* **79**, 415 (1996).
63. U. Becker, *J. Electron Spectrosc. Relat. Phenom.* **112**, 47 (2000).
64. J. H. D. Eland, M. Takahashi and Y. Hikosaka, *Faraday Discuss.* **115**, 119 (2000).
65. Y. Hikosaka and J. H. D. Eland, *Phys. Chem. Chem. Phys.* **2**, 4663 (2000).
66. Y. Hikosaka and J. H. D. Eland, *J. Phys. B-At. Mol. Opt. Phys.* **33**, 3137 (2000).
67. Y. Hikosaka, J. H. D. Eland, T. M. Watson and I. Powis, *J. Chem. Phys.* **115**, 4593 (2001).
68. Y. Hikosaka and J. H. D. Eland, *Chem. Phys.* **277**, 53 (2002).
69. A. Lafosse, M. Lebech, J. C. Brenot, P. M. Guyon, O. Jagutzki, L. Spielberger, M. Vervloet, J. C. Houver and D. Dowek, *Phys. Rev. Lett.* **84**, 5987 (2000).
70. A. Lafosse, J. C. Brenot, A. V. Golovin, P. M. Guyon, K. Hoejrup, J. C. Houver, M. Lebech and D. Dowek, *J. Chem. Phys.* **114**, 6605 (2001).
71. D. Dowek, J. C. Brenot, P. M. Guyon, J. C. Houver, A. Lafosse, M. Lebech, O. Jagutzki and L. Spielberger, *Nucl. Instrum. Methods Phys. Res. Sect. A-Accel. Spectrom. Dect. Assoc. Equip.* **477** 323 (2002).

72. O. Gessner, Y. Hikosaka, B. Zimmermann, A. Hempelmann, R. R. Lucchese, J. H. D. Eland, P. M. Guyon and U. Becker, *Phys. Rev. Lett.* **88**, 193002 (2002).
73. M. Lebech, J. C. Houver and D. Dowek, *Rev. Sci. Instr.* **73**, 1866 (2002).
74. R. R. Lucchese, A. Lafosse, J. C. Brenot, P. M. Guyon, J. C. Houver, M. Lebech, G. Raseev and D. Dowek, *Phys. Rev.* **A65**, 020702 (2002).
75. I. Powis, *J. Chem. Phys.* **99**, 3436 (1993).
76. I. Powis, *J. Chem. Phys.* **103**, 5570 (1995).
77. I. Powis, *J. Chem. Phys.* **106**, 5013 (1997).
78. P. Downie and I. Powis, *Faraday Discuss.* 103 (2000).
79. J. B. Milan, W. J. Buma and C. A. de Lange, *J. Chem. Phys.* **105**, 6688 (1996).
80. C. A. de Lange, *J. Chem. Soc.-Faraday Trans.* **94**, 3409 (1998).
81. A. Hiraya, Y. Achiba, K. Kimura and E. C. Lim, *Chem. Phys. Lett.* **185**, 303 (1991).
82. B. Kim, C. P. Schick and P. M. Weber, *J. Chem. Phys.* **103**, 6903 (1995).
83. V. Blanchet, M. Z. Zgierski, T. Seideman and A. Stolow, *Nature* **401**, 52 (1999).
84. V. Blanchet, M. Z. Zgierski and A. Stolow, *J. Chem. Phys.* **114**, 1194 (2001).
85. M. Schmitt, S. Lochbrunner, J. P. Shaffer, J. J. Larsen, M. Z. Zgierski and A. Stolow, *J. Chem. Phys.* **114**, 1206 (2001).
86. J. B. Pallix and S. D. Colson, *Chem. Phys. Lett.* **119**, 38 (1985).
87. E. Sekreta and J. P. Reilly, *Chem. Phys. Lett.* **149**, 482 (1988).
88. P. M. Weber and N. Thantu, *Chem. Phys. Lett.* **197**, 556 (1992).
89. C. P. Schick, S. D. Carpenter and P. M. Weber, *J. Phys. Chem.* **A103**, 10470 (1999).
90. X. B. Song, C. W. Wilkerson, J. Lucia, S. Pauls and J. P. Reilly, *Chem. Phys. Lett.* **174**, 377 (1990).
91. J. M. Smith, C. Lakshminarayan and J. L. Knee, *J. Chem. Phys.* **93**, 4475 (1990).
92. D. E. Powers, J. B. Hopkins and R. E. Smalley, *J. Chem. Phys.* **72**, 5721 (1980).
93. J. S. Baskin, M. Dantus and A. H. Zewail, *Chem. Phys. Lett.* **130**, 473 (1986).
94. K. Muller-Dethlefs, E. W. Schlag, E. R. Grant, K. Wang and V. Mckoy, *Adv. Chem. Phys.* **XC**, 104 (1995).
95. K. Muller-Dethlefs, in *High Resolution Laser Photoionization and Photoelectron Studies*, eds. I. Powis, T. Baer and C. Y. Ng (John Wiley, Chichester, 1995), p. 21.
96. E. W. Schlag, *ZEKE spectroscopy* (Cambridge University Press, 1998).
97. M. J. Cote, J. F. Kauffman, P. G. Smith and J. D. McDonald, *J. Chem. Phys.* **90**, 2865 (1989).
98. J. F. Kauffman, M. J. Cote, P. G. Smith and J. D. McDonald, *J. Chem. Phys.* **90**, 2874 (1989).
99. J. M. Smith, X. Zhang and J. L. Knee, *J. Chem. Phys.* **99**, 2550 (1993).
100. J. M. Smith, X. Zhang and J. L. Knee, *J. Phys. Chem.* **99**, 1768 (1995).

101. M. R. Dobber, W. J. Buma and C. A. de Lange, *J. Chem. Phys.* **99**, 836 (1993).
102. M. R. Dobber, W. J. Buma and C. A. de Lange, *J. Phys. Chem.* **99**, 1671 (1995).
103. T. Schultz and I. Fischer, *J. Chem. Phys.* **107**, 8197 (1997).
104. T. Schultz and I. Fischer, *J. Chem. Phys.* **109**, 5812 (1998).
105. M. Seel and W. Domcke, *Chem. Phys.* **151**, 59 (1991).
106. R. Schneider and W. Domcke, *Chem. Phys. Lett.* **150**, 235 (1988).
107. L. Seidner, G. Stock, A. L. Sobolewski and W. Domcke, *J. Chem. Phys.* **96**, 5298 (1992).
108. W. Domcke, A. L. Sobolewski and C. Woywod, *Chem. Phys. Lett.* **203**, 220 (1993).
109. C. Woywod, W. Domcke, A. L. Sobolewski and H. J. Werner, *J. Chem. Phys.* **100**, 1400 (1994).
110. S. Hahn and G. Stock, *Phys. Chem. Chem. Phys.* **3**, 2331 (2001).
111. V. Stert, P. Farmanara and W. Radloff, *J. Chem. Phys.* **112**, 4460 (2000).
112. D. R. Cyr and C. C. Hayden, *J. Chem. Phys.* **104**, 771 (1996).
113. T. S. Rose, M. J. Rosker and A. H. Zewail, *J. Chem. Phys.* **88**, 6672 (1988).
114. T. S. Rose, M. J. Rosker and A. H. Zewail, *J. Chem. Phys.* **91**, 7415 (1989).
115. M. J. Rosker, M. Dantus and A. H. Zewail, *J. Chem. Phys.* **89**, 6113 (1988).
116. C. Meier and V. Engel, *Chem. Phys. Lett.* **212**, 691 (1993).
117. Y. Arasaki, K. Takatsuka, K. Wang and V. Mckoy, *Chem. Phys. Lett.* **302**, 363 (1999).
118. Y. Arasaki, K. Takatsuka, K. Wang and V. McKoy, *J. Chem. Phys.* **112**, 8871 (2000).
119. Y. Arasaki, K. Takatsuka, K. Wang and V. McKoy, *J. Chem. Phys.* **114**, 7941 (2001).
120. K. Takatsuka, Y. Arasaki, K. Wang and V. McKoy, *Faraday Discuss.* **115**, 1 (2000).
121. T. Baumert, R. Thalweiser and G. Gerber, *Chem. Phys. Lett.* **209**, 29 (1993).
122. A. Assion, M. Geisler, J. Helbing, V. Seyfried and T. Baumert, *Phys. Rev.* **A54**, R4605 (1996).
123. I. Fischer, D. M. Villeneuve, M. J. Vrakking and A. Stolow, *J. Chem. Phys.* **102**, 5566 (1995).
124. I. Fischer, M. J. Vrakking, D. M. Villeneuve and A. Stolow, *Chem. Phys.* **207**, 331 (1996).
125. J. A. Syage, *Chem. Phys. Lett.* **202**, 227 (1993).
126. J. A. Syage, *J. Phys. Chem.* **99**, 5772 (1995).
127. R. Lopezmartens, P. Long, D. Solgadi, B. Soep, J. Syage and P. Millie, *Chem. Phys. Lett.* **273**, 219 (1997).
128. S. Lochbrunner, T. Schultz, M. Schmitt, J. P. Shaffer, M. Z. Zgierski and A. Stolow, *J. Chem. Phys.* **114**, 2519 (2001).
129. V. Blanchet and A. Stolow, *J. Chem. Phys.* **108**, 4371 (1998).
130. B. J. Greenblatt, M. T. Zanni and D. M. Neumark, *Chem. Phys. Lett.* **258**, 523 (1996).

131. M. T. Zanni, V. S. Batista, B. J. Greenblatt, W. H. Miller and D. M. Neumark, *J. Chem. Phys.* **110**, 3748 (1999).
132. M. T. Zanni, T. R. Taylor, B. J. Greenblatt, B. Soep and D. M. Neumark, *J. Chem. Phys.* **107**, 7613 (1997).
133. M. T. Zanni, A. V. Davis, C. Frischkorn, M. Elhanine and D. M. Neumark, *J. Chem. Phys.* **112**, 8847 (2000).
134. B. J. Greenblatt, M. T. Zanni and D. M. Neumark, *Science* **276**, 1675 (1997).
135. B. J. Greenblatt, M. T. Zanni and D. M. Neumark, *J. Chem. Phys.* **111**, 10566 (1999).
136. B. J. Greenblatt, M. T. Zanni and D. M. Neumark, *Faraday Discuss.* 101 (1997).
137. B. J. Greenblatt, M. T. Zanni and D. M. Neumark, *J. Chem. Phys.* **112**, 601 (2000).
138. M. T. Zanni, B. J. Greenblatt and D. M. Neumark, *J. Chem. Phys.* **109**, 9648 (1998).
139. M. T. Zanni, B. J. Greenblatt, A. V. Davis and D. M. Neumark, *J. Chem. Phys.* **111**, 2991 (1999).
140. M. T. Zanni, C. Frischkorn, A. V. Davis and D. M. Neumark, *J. Phys. Chem.* **A104**, 2527 (2000).
141. L. Lehr, M. T. Zanni, C. Frischkorn, R. Weinkauf and D. M. Neumark, *Science* **284**, 635 (1999).
142. A. V. Davis, M. T. Zanni, C. Frischkorn and D. M. Neumark, *J. Electron Spectrosc. Relat. Phenom.* **108**, 203 (2000).
143. C. Frischkorn, M. T. Zanni, A. V. Davis and D. M. Neumark, *Faraday Discuss.* **115**, 49 (2000).
144. D. H. Paik, T. M. Bernhardt, N. J. Kim and A. H. Zewail, *J. Chem. Phys.* **115**, 612 (2001).
145. V. Stert, W. Radloff, C. P. Schulz and I. V. Hertel, *Eur. Phys. J.* **D5**, 97 (1999).
146. W. Radloff, in *Photoionization and photodetachment*, ed. C. Y. Ng (World Scientific, Singapore, 1999), p. 127.
147. S. Wolf, G. Sommerer, S. Rutz, E. Schreiber, T. Leisner and L. Wöste, *Phys. Rev. Lett.* **74**, 4177 (1995).
148. L. Wöste, *Z. Phys. Chemie-Int. J. Res. Phys. Chem. Chem. Phys.* **196**, 1 (1996).
149. D. W. Boo, Y. Ozaki, L. H. Andersen and W. C. Lineberger, *J. Phys. Chem.* **A101**, 6688 (1997).
150. S. Rutz, H. Ruppe, E. Schreiber and L. Wöste, *Z. Phys. D-At. Mol. Clusters* **40**, 25 (1997).
151. T. Leisner, S. Vajda, S. Wolf, L. Woste and R. S. Berry, *J. Chem. Phys.* **111**, 1017 (1999).
152. L. Wöste, *Opt. Appl.* **29**, 543 (1999).
153. H. Hess, S. Kwiet, L. Socaciu, S. Wolf, T. Leisner and L. Wöste, *Appl. Phys. B-Lasers Opt.* **71**, 337 (2000).
154. H. Hess, K. R. Asmis, T. Leisner and L. Wöste, *Eur. Phys. J.* **D16**, 145 (2001).

155. V. Stert, W. Radloff, H. H. Ritze and T. Freudenberg, *Chem. Phys. Lett.* **204**, 287 (1993).
156. V. Stert, W. Radloff, T. Freudenberg, F. Noack, I. V. Hertel, C. Jouvet, C. Dedonderlardeux and D. Solgadi, *Europhys. Lett.* **40**, 515 (1997).
157. P. Farmanara, W. Radloff, V. Stert, H. H. Ritze and I. V. Hertel, *J. Chem. Phys.* **111**, 633 (1999).
158. R. Farmanara, H. H. Ritze, V. Stert, W. Radloff and I. V. Hertel, *J. Chem. Phys.* **116**, 1443 (2002).
159. P. Farmanara, V. Stert, W. Radloff and I. V. Hertel, *J. Phys. Chem.* **A105**, 5613 (2001).
160. V. Stert, H. H. Ritze, E. T. J. Nibbering and W. Radloff, *Chem. Phys.* **272**, 99 (2001).
161. R. E. Continetti, *Int. Rev. Phys. Chem.* **17**, 227 (1998).
162. R. E. Continetti, *Ann. Rev. Phys. Chem.* **52**, 165 (2001).
163. V. Stert, P. Farmanara, W. Radloff, F. Noack, S. Skowronek, J. Jimenez and A. G. Urena, *Phys. Rev.* **A59**, R1727 (1999).
164. W. C. Wiley and I. H. Mclaren, *Rev. Sci. Instr.* **60**, 1150 (1955).
165. E. Wrede, S. Laubach, S. Schulenburg, A. J. Orr-Ewing and M. N. R. Ashfold, *Chem. Phys. Lett.* **326**, 22 (2000).
166. E. Wrede, S. Laubach, S. Schulenburg, A. Brown, E. R. Wouters, A. J. Orr-Ewing and M. N. R. Ashfold, *J. Chem. Phys.* **114**, 2629 (2001).
167. D. W. Chandler, J. W. Thoman, M. H. M. Janssen and D. H. Parker, *Chem. Phys. Lett.* **156**, 151 (1989).
168. P. L. Houston, *Acc. Chem. Res.* **28**, 453 (1995).
169. B. J. Whitaker, in *Research in Chemical Kinetics*, eds. R. G. Compton and G. Hancock (Elsevier, Amsterdam, 1993), p. 307.
170. B. J. Whitaker, in *Imaging in Chemical Dynamics*, eds. A. G. Suits and R. E. Continetti (American Chemical Society, Washington, D.C., 2000), p. 68.
171. Y. Sato, Y. Matsumi, M. Kawasaki, K. Tsukiyama and R. Bersohn, *J. Phys. Chem.* **99**, 16307 (1995).
172. M. J. J. Vrakking, *Rev. Sci. Instr.* **72**, 4084 (2001).
173. V. Dribinski, A. Ossadtchi, V. Mandelshtam and H. Reisler, *Rev. Sci. Instr.*, submitted (2002).
174. H. Katayanagi, Y. Matsumoto, M. Tsubouchi, T. Suzuki and C. A. de Lange, *J. Chem. Phys.* in press.
175. G. Sha, D. Proch, C. Rose and K. L. Kompa, *J. Chem. Phys.* **99**, 4334 (1993).
176. C. P. Schick and P. M. Weber, *J. Phys. Chem.* **A105**, 3725 (2001).
177. C. P. Schick and P. M. Weber, *J. Phys. Chem.* **A105**, 3735 (2001).
178. C. N. Yang, *Phys. Rev.* **74**, 764 (1948).
179. R. Bersohn and S. H. Lin, *Adv. Chem. Phys.* **16**, 80 (1969).
180. R. N. Zare, *Mol. Photochem.* **4**, 1 (1972).
181. M. P. Strand, J. Hansen, R.-L. Chien and R. S. Berry, *Chem. Phys. Lett.* **59**, 205 (1978).
182. G. Leuchs, S. J. Smith, E. Khawaja and H. Walther, *Opt. Commun.* **31**, 313 (1979).

183. P. M. Felker and A. H. Zewail, *J. Chem. Phys.* **86**, 2460 (1987).
184. J. S. Baskin, P. M. Felker and A. H. Zewail, *J. Chem. Phys.* **86**, 2483 (1987).
185. P. M. Felker and A. H. Zewail, in *Femtochemistry*, eds. J. Manz and L. Woste (VCH publishing, New York, 1994), p. 193.
186. P. M. Felker and A. H. Zewail, in *Jet Spectroscopy and Molecular Dynamics*, eds. J. M. Hollas and D. Phillips (Blackie Academic and Professional, Glasgow, 1995), p. 181.
187. P. M. Felker and A. H. Zewail, in *Jet Spectroscopy and Molecular Dynamics*, eds. J. M. Hollas and D. Phillips (Blackie Academic and Professional, Glasgow, 1995), p. 222.
188. P. Debye, *Polar Molecules* (Chemical Catalog Company, New York, 1929).
189. F. Perrin, *J. Phys. Radium* **5**, 497 (1934).
190. F. Perrin, *J. Phys. Radium* **7**, 1 (1936).
191. K. B. Eisenthal, *Acc. Chem. Res.* **8**, 118 (1975).
192. W. A. Steele, *J. Chem. Phys.* **38**, 2404 (1962).
193. W. A. Steele, *J. Chem. Phys.* **38**, 2411 (1962).
194. J. S. Baskin, M. Gupta, M. Chachisvilis and A. H. Zewail, *Chem. Phys. Lett.* **275**, 437 (1997).
195. J. S. Baskin, M. Chachisvilis, M. Gupta and A. H. Zewail, *J. Phys. Chem.* **A102**, 4158 (1998).
196. J. S. Baskin and A. H. Zewail, *J. Phys. Chem.* **A105**, 3680 (2001).
197. C. Jonah, *J. Chem. Phys.* **55**, 1915 (1971).
198. S.-C. Yang and R. Bersohn, *J. Chem. Phys.* **61**, 4400 (1974).
199. R. Bersohn, *Isr. J. Chem.* **14**, 111 (1975).
200. K. L. Reid and J. G. Underwood, *J. Chem. Phys.* **112**, 3643 (2000).
201. J. G. Underwood and K. L. Reid, *J. Chem. Phys.* **113**, 1067 (2000).
202. S. C. Althorpe and T. Seideman, *J. Chem. Phys.* **110**, 147 (1999).
203. C. Riehn, A. Weichert and B. Brutschy, *Phys. Chem. Chem. Phys.* **2**, 1873 (2000).
204. A. Frad, F. Lahmani, A. Tramer and C. Tric, *J. Chem. Phys.* **60**, 4419 (1974).
205. F. Lahmani, A. Tramer and C. Tric, *J. Chem. Phys.* **60**, 4431 (1974).
206. M. Bixon and J. Jortner, *J. Chem. Phys.* **48**, 715 (1968).
207. P. Avouris, W. M. Gelbert and M. A. El-Sayed, *Chem. Rev.* **77**, 793 (1977).
208. D. B. Mcdonald, G. R. Fleming and S. A. Rice, *Chem. Phys.* **60**, 335 (1981).
209. S. Okajima, H. Saigusa and E. Lim, *J. Chem. Phys.* **76**, 2096 (1982).
210. I. Yamazaki, T. Murao, T. Yamanaka and K. Yoshihara, *Faraday Discuss.* 395 (1983).
211. A. Lorincz, D. D. Smith, F. Novak, R. Kosloff, D. J. Tannor and S. A. Rice, *J. Chem. Phys.* **82**, 1067 (1985).
212. J. L. Knee, F. E. Doany and A. H. Zewail, *J. Chem. Phys.* **82**, 1042 (1985).
213. P. M. Felker and A. H. Zewail, *Chem. Phys. Lett.* **128**, 221 (1986).
214. B. J. Van Der Meer, H. T. Jonkman, J. Kommandeur, W. L. Meerts and W. A. Majewski, *Chem. Phys. Lett.* **92**, 565 (1982).
215. P. J. de Lange, K. E. Drabe and J. Kommandeur, *J. Chem. Phys.* **84**, 538 (1986).

216. L. Zhu and P. Johnson, *J. Chem. Phys.* **99**, 2322 (1993).
217. T. G. Dietz, M. A. Duncan, A. C. Pulu and R. E. Smalley, *J. Phys. Chem.* **86**, 4026 (1982).
218. S. Hillenbrand, L. Zhu and P. Johnson, *J. Chem. Phys.* **92**, 870 (1990).
219. S. Hillenbrand, L. Zhu and P. Johnson, *J. Chem. Phys.* **95**, 2237 (1991).
220. H. A. Bethe, *Handbuch der Physik* (Springer-Verlag, Berlin, 1933), p. 483.
221. J. Cooper and R. N. Zare, *J. Chem. Phys.* **48**, 942 (1968).
222. K. K. Innes, I. G. Ross and W. R. Moomaw, *J. Mol. Spectrosc.* **132**, 492 (1988).
223. L. Seidner, W. Domcke and W. Vonniessen, *Chem. Phys. Lett.* **205**, 117 (1993).
224. T. Seideman, *J. Chem. Phys.* **113**, 1677 (2000).
225. T. Seideman, *Phys. Rev.* **A64**, 42504 (2001).
226. D. Dill, *J. Chem. Phys.* **65**, 1130 (1976).
227. D. Dill, J. Siegel and J. L. Dehmer, *J. Chem. Phys.* **65**, 3158 (1976).
228. S. W. Allendorf, D. J. Leahy, D. C. Jacobs and R. N. Zare, *J. Chem. Phys.* **91**, 2216 (1989).
229. D. J. Leahy, K. L. Reid and R. N. Zare, *J. Phys. Chem.* **95**, 8154 (1991).
230. D. J. Leahy, K. L. Reid and R. N. Zare, *J. Chem. Phys.* **95**, 1757 (1991).
231. K. L. Reid, D. J. Leahy and R. N. Zare, *J. Chem. Phys.* **95**, 1746 (1991).
232. D. J. Leahy, K. L. Reid, H. K. Park and R. N. Zare, *J. Chem. Phys.* **97**, 4948 (1992).
233. K. L. Reid, D. J. Leahy and R. N. Zare, *Phys. Rev. Lett.* **68**, 3527 (1992).
234. K. L. Reid and D. J. Leahy, in *High Resolution Laser Photoionization and Photoelectron Studies*, eds. I. Powis, T. Baer and C. Ng (John Wiley and Sons, 1995), p. 247.
235. S. N. Dixit, D. L. Lynch, V. Mckoy and W. M. Huo, *Phys. Rev.* **A32**, 1267 (1985).
236. H. Rudolph and V. McKoy, *J. Chem. Phys.* **91**, 2235 (1989).
237. X. B. Song, E. Sekreta, J. P. Reilly, H. Rudolph and V. McKoy, *J. Chem. Phys.* **91**, 6062 (1989).
238. K. Wang and V. McKoy, in *High Resolution Laser photoionization and Photoelectron Studies*, eds. I. Powis, T. Baer and C. Ng (John Wiley and Sons, 1995), p. 281.
239. C. F. Dion and E. R. Bernstein, *J. Chem. Phys.* **103**, 4907 (1995).
240. M. Hentschel, R. Kienberger, C. Spielmann, G. A. Reider, N. Milosevic, T. Brabec, P. Corkum, U. Heinzmann, M. Drescher and F. Krausz, *Nature* **414**, 509 (2001).
241. M. Drescher, M. Hentschel, R. Kienberger, G. Tempea, C. Spielmann, G. A. Reider, P. B. Corkum and F. Krausz, *Science* **291**, 1923 (2001).

CHAPTER 13

MANIPULATING COLD MOLECULES WITH NONRESONANT FIELDS

Bretislav Friedrich

Department of Chemistry and Chemical Biology and Department of Physics, Harvard University, Cambridge, MA 02138, U.S.A.

Contents